Journal of South American Earth Sciences 43 (2013) 127–144

Contents lists available at SciVerse ScienceDirect

Journal of South American Earth Sciences

journal homepage: www.elsevier.com/locate/jsames

Dynamic topography in South America

Federico M. Dávila [a,b,*], Carolina Lithgow-Bertelloni [a]

[a] Earth Sciences, University College London, Gower Street, London WC1E 6BT, United Kingdom
[b] CICTERRA – CONICET, Universidad Nacional de Cordoba, Av. V. Sarsfield 1611, Cordoba 5016, Argentina

ARTICLE INFO

Article history:
Received 31 March 2012
Accepted 17 December 2012

Keywords:
Dynamic topography
Basin analysis
Eastern Venezuela Basins
Amazon foreland
Fitzcarrald Arch
Sierras Pampeanas
Argentine Pampas
Patagonia
Argentine abyssal Basin

ABSTRACT

Supracrustal tectonics and mantle flow interact to create Earth's topography. While tectonics is associated with the isostatic components of topography, the deflections caused by mantle dynamics, or dynamic topography, represent the non-isostatic components. South America is an ideal natural laboratory to analyze these two contrasting components from the high Andes to the distal plains. Both regions are active and affected by complex geodynamic processes like the subduction of oceanic ridges, geometry and age of slabs, etc. These subducting anomalies affect not only the convergence dynamics and stresses along the entire margin, but also the distribution of mass anomalies in the mantle, which are the main cause of sublithospheric flow and dynamic topography. Here we revisited five examples from north to south, which demonstrate that, the Andes and the distal forelands have been uncompensated since the beginning of the Cenozoic and that additional forces, such as mantle downwellings and upwellings, are required to account for the observed topographies in basins and elevations.

1. Introduction

Earth's large-scale topography is the result of local to regional flexural isostatic adjustment to variations in lithospheric structure and surface loading, overlapped by the dynamic stresses transmitted to the Earth's surface resulting from subsurface buoyancy variations induced by mantle flow (Fig. 1a). While the isostatic and flexural components of topography occur over shorter wavelengths of ≤300 km (García-Castellanos et al., 1997), the long-wavelength components act generally over hundreds of kilometers (>300 km) and are controlled by the density and rheological structure of the mantle. The overlapping of tectonically driven isostatic adjustment and mantle dynamics creates most of topographic signals observed in the landscape or captured from space from satellite missions (e.g., DEMs). The positive large-scale (long-wavelength) vertical motion of the Earth surface has been generically defined as epeirogenesis and could be related to the "surface uplift" term of England and Molnar (1990). The negative vertical displacement, in turn, can be associated with the "intra- or peri- cratonic subsidence" term of Cross and Pilger (1978).

South America is an ideal natural laboratory to analyze these components of the topography. From the high Andes to the most distal plains, and since Andean orogeny in the late Cretaceous; supracrustal and sublithospheric processes have been affected by changes in the convergence rates, subducting slab age, slab-dip angle, and lithospheric thickening or thinning (Ramos, 2009). The western margin, in fact, has been affected by subduction of oceanic ridges (e.g., Yañez et al., 2001) since the early Cenozoic (Kay and Mpodozis, 2002), which modified not only the stress fields (and upper plate deformation) but also the density distribution in the asthenospheric wedge.

Here we demonstrate that: (1) the Andes (from the High Cordillera to the most distal foreland) were mostly uncompensated (over- and under-compensated) throughout the Cenozoic, and that (2) additional forces, like mantle downwelling and upwelling, are required to account for the observed topographies (basins and elevations). We organized this contribution in four main sections: (1) General concepts, (2) physics and numerical formulations behind dynamic topography, (3) previous studies at global and regional scales, and (4) new results. In the discussion and conclusions, we highlight future perspectives for dynamic topography studies in South America. We show that different topographic anomalies might be associated with mantle processes and that their study provides unique avenues to improve our understanding of mantle dynamics.

2. Dynamic topography

According to Archimedes principle any mass floating on a fluid is supported, or compensated, by a deep root. If the material is less

* Corresponding author. Earth Sciences, University College London, Gower Street, London WC1E 6BT, United Kingdom.
E-mail address: f.davila@ucl.ac.uk (F.M. Dávila).

0895-9811/$ – see front matter © 2013 Elsevier Ltd. All rights reserved.
http://dx.doi.org/10.1016/j.jsames.2012.12.002

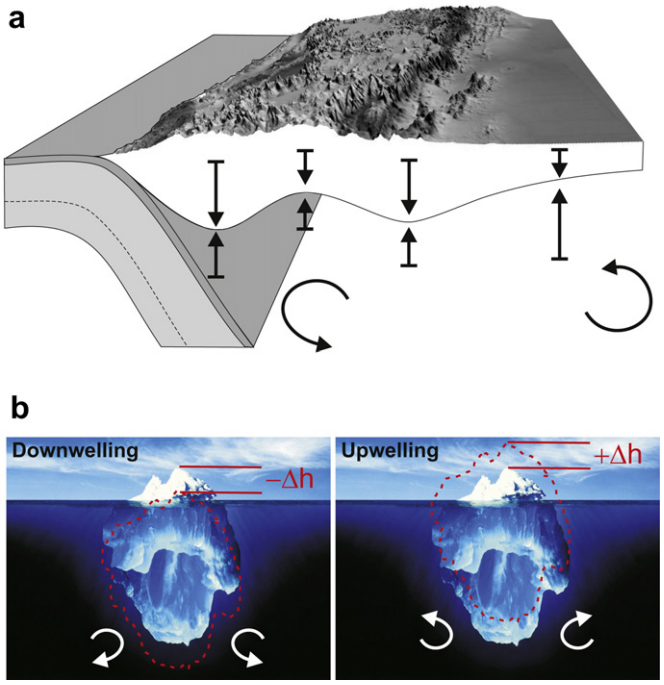

Fig. 1. (a) Forces affecting the topographic signal of the Earth's surface. The vertical arrows represent the lithospheric loads (downward) and compensations forces from the mantle (upward). Note that there is a correspondence between the vertical stresses and lithospheric thicknesses. The curved arrows represent the mantle flow driven by the subducting slab (dark grey is the oceanic crust and light grey is the oceanic lithosphere). (b) Icerberg picture showing dynamic topography (Δh) associated to the dynamics of seawater flow (curved arrows). The positive changes ($+\Delta h$) are dynamic uplift, linked to upwellings, and the negatives ($-\Delta h$) to dynamic subsidence, associated to downwellings.

dense than the fluid it floats with a "root" below the surface, which is proportional to the entity contrast between the two materials (e.g. ice in water). This concept, known as isostasy in geology, implies the existence of a constant–pressure compensation level, usually the point at which the mantle starts flowing. However, static and constant-pressure surfaces are difficult to constrain because a depth of compensation is controlled by the thickness, density and rheological structure of the lithosphere, which are not fully understood (see Stixrude and Lithgow-Bertelloni, 2005).

We define the dynamic contribution on any topography, known as "dynamic topography" (Richards and Hager, 1984), as the net displacement of the Earth surface in response to flow (Fig. 1b). The deflection is caused by the vertical stresses arising from viscous flow in the mantle in response to its 3-D density structure. As in simple Airy isostasy, the amplitude is inversely proportional to the inherent density contrast across the boundary (i.e. lithosphere-air or lithosphere-ocean) however; it is also directly proportional to the magnitude of the stresses impinging on the surface ($h = -$Trr/deltarho*g). Because it is a direct result of the stresses deflecting the surface the buoyancy source generating the flow may be far removed from the bottom of the lithosphere. In other words, it is distinctly different than advocating a sub-lithospheric density anomaly (such as partial melt), whose effects are more akin to isostasy.

At long-wavelength scales, dynamic topography is the most important contributor to Earth's topography (Ricard et al., 2006) both on the continents (Lithgow-Bertelloni and Silver, 1998; Daradich et al., 2003) and in the oceans (Cazenave and Thoraval, 1994; Conrad et al., 2004). Dynamic topography has also been considered the main mechanism for generating the anomalous thicknesses in deep sedimentary basins (Pysklywec and Mitrovica, 1999; Burgess et al., 1997) as well as an important control on the surface deformation and present state of stress of the lithosphere in areas of long-lived subduction such as Southeast Asia (Lithgow-Bertelloni and Guynn, 2004) and the Americas (Liu et al., 2008). Mantle forces might also cause tilting of entire continents (Mitrovica et al., 1989; Gurnis, 1990) and influence on the shape of the ocean surface via its effect on the geoid. Some recent evidence also suggests that dynamic topography may act at shorter wavelengths (Hartley et al., 2011; Moucha and Forte, 2011).

The relationship between mantle dynamics and topography is direct and instantaneous. As a plate migrates over a mantle upwelling or downwelling, large vertical motions lead to the emergence or submergence, respectively (positive and negative dynamic topographies, Lithgow-Bertelloni and Gurnis, 1997). In North America, across the Western Interior Basins, the Cretaceous-Early Cenozoic subsidence and subsequent Miocene uplifting has been associated with changes in the mantle flow driven by subduction dynamics (Mitrovica et al., 1989; Liu et al., 2008). While flat subduction was connected to widespread-deep subsidence stages, dipping subduction systems to more localized subsidence and non-subduction to uplift (Mitrovica et al., 1989; Liu et al., 2008). However, the North American example is ancient, thus evidence is drawn from the geologic record and important geophysical from subduction geometries, mantle properties and tectonic features are inferred. From the subduction geometries, mantle properties to the basin and tectonic features have been inferred (e.g., Liu et al., 2008). South America, in contrast, represents a better analogue and natural lab to test the connections between mantle dynamics and topography given that it has been an active subducting margin since likely the Paleozoic (see Dávila, 2003). This region certainly has fewer assumptions, especially when it is compared to fossil examples. There are several geophysical studies to characterize the lithosphere and mantle composition as well as geological and geophysical observations on sub-recent to present day records.

3. Computing dynamic topography

Mantle flow models are based on solutions to the governing equations for the conservation of mass, momentum (non-inertial) and energy (advection and diffusion with sources from radioactive decay) together with constitutive relations for rheology abstracted from laboratory measurements and theoretical considerations. Such models have shown that, while the mantle behaves rigidly on short time scales, for example in the propagation of seismic shear waves, it behaves like a fluid on long time scales ($<10^4$ years). Most heat is transported to the surface by large-scale solid-state convective flow, with typical overturn times of 100 my. A number of geophysical observables can be predicted from these solutions, including dynamic topography, geoid, and seismic structure.

While the equations have been known for centuries and numerical solutions abound, the problem for the plate-mantle system lies in identifying the proper constitutive relation, i.e. the rheology of mantle and lithospheric materials. Obtaining the appropriate law that captures both plate boundary behavior and internal dynamics and accounts for the large range of conditions in pressure, temperature, composition and stress in the Earth has proven difficult (e.g., Liu and Gurnis, 2008). It is possible to solve the equations numerically from first principles with a given rheological law to study the fluid dynamics of the system and much has been learned in the last two decades (Tackley et al., 1993). However, such models cannot, without knowledge of the initial conditions and all contingencies of Earth history, reproduce a present-day Earth for direct comparison to geological observations. One strategy is to impose the plate motion history (Han and Gurnis, 1999; Liu and Gurnis, 2008) for the last 100–200 my, combined with adjoint models and data assimilation the latter can potentially allow for very

sophisticated comparisons to observations (Liu et al., 2008; Shephard et al., 2010). Numerical computations, particularly adjoint models are numerically intensive and do not easily allow for a full exploration of parameter space. They can be limited by the choice or availability of seismic tomographic models for a guess at the initial state of mantle structure. And, while resolution has greatly improved, they cannot capture at present, the large variations along strike in slab morphology and density structure present in the South America slab. Instead, to capture such variations and analyze the impact of slab morphology and density structure on dynamic topography, we take a simpler approach. Rather than solving the coupled energy, momentum and mass conservation equations numerically, we solve only for the conservation of mass and momentum analytically to an arbitrary resolution (Hager and O'Connell, 1981). The key approximations are choosing a Newtonian rheology and assuming knowledge of the 3-D density heterogeneity in the mantle (Hager et al., 1985). For the latter one may use seismic tomographic models (living with the consequences of their uncertainties and resolution) to construct models based on the history of subduction (Ricard et al., 1993; Lithgow-Bertelloni and Richards, 1998; Dávila and Lithgow-Bertelloni, 2011) or the present-day structure of the South American slab (e.g., Dávila et al., 2010; Dávila and Lithgow-Bertelloni, 2011). With those approximations one solves for the instantaneous viscous flow induced in the mantle by the presence of mass anomalies and can compute geophysical observables such as the geoid and dynamic topography.

4. Global models

On the basis of the instantaneous flow formulation of Hager and O'Connell (1981) and the hypsometric curves of Harrison et al. (1983), Lithgow-Bertelloni and Gurnis (1997) examined the Cenozoic vertical motion of South America since ~65 Ma to Present day. The flow model to calculate dynamic topography was constructed with sub-vertical subducting slabs, a lower mantle 10 and 50 times less viscous with respect to the lithosphere and upper mantle, respectively; and a density contrast mantle-slab of ~80 kg/m^3 (Lithgow-Bertelloni and Gurnis, 1997). The results showed a several hundred meter discrepancy (Fig. 2) in South America, likely the largest on Earth, attributed to the tectonic reconstructions and assumptions on the rotation vector of the Phoenix (Aluk) plate. But the compiled hypsometry were also likely not fully correct. Considering sea incursions affected South America during the Cenozoic (e.g., Ruskin et al., 2011 and references therein), it is quite difficult to reconcile a differential vertical motion of only 60 m as predicted by existing hypsometry (Harrison et al., 1983). In fact, recent studies on Quaternary marine terraces along the Atlantic margin of Argentina have shown differences in elevations of >100 m (Pedoja et al., 2011). The assumed slab structure in the model would be problematic as well at least for South America, regardless of the plate reconstructions. No sub-vertical slabs have been inferred from geological approaches for the entire South American margin since the early Cenozoic (Ramos, 2009).

But later work, based on seismic tomography and occasionally more sophisticated rheology, arrived at the same results (Steinberger, 2007; Heine et al., 2008; Conrad and Husson, 2009; among others). South America would seem to rest, according to these studies, on a continental-scale mantle downwelling cell since it separated from Africa in the Cretaceous. This, as shown by most global models, would generate continental-scale dynamic subsidence. Those studies rely on seismic tomographic models, which see the presence of the Nazca slab under South America but do not and cannot capture its variations in morphology and density structure. However, the latter is critical. Because, as we will show in the next chapter, the changes in topography in South America were not uniform, instead they are marked by fluctuating episodes of uplift-subsidence, and strongly influenced by a changing tectonic-dynamic scenario (Ramos, 2009).

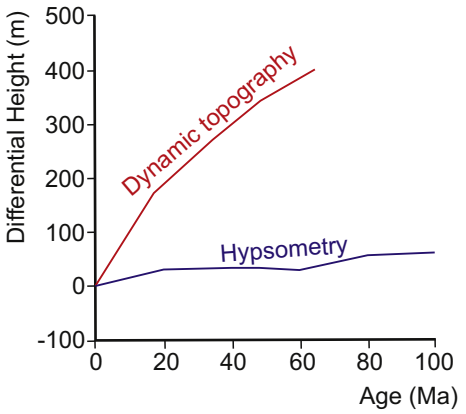

Fig. 2. Comparison between the dynamic topography and hypsometry of South America. The red curve shows the modeled differential vertical motion (dynamic topography) of South America (after Lithgow-Bertelloni and Gurnis, 1997) since ~100 Ma. The hypsometric curve (blue) by Harrison et al. (1983). Note that there is a remarkable gap between modeling and geological studies.

5. Regional models

5.1. The Eastern Venezuela foreland

In northernmost South America, between 13° and 7° NL and 66°–60° WL, we find the Maturín basin (Jácome et al., 2003a, b) (Fig. 3), which has a Miocene-Present foreland sedimentary record locally >10 km thick. The basin was first interpreted as a flexural depositional foreland generated by the loading of the Serrania and the Monagas thrust belts (Roure et al., 1994; Chevalier et al., 1995; Passalacqua et al., 1995; Hung, 1997). The mean orogenic shortening was estimated at ~80 km. However, the whole shortening, associated with the basin formation, decreases from west (96 km) to east (76 km), (Jácome et al., 2003a), whereas the sedimentary thicknesses decrease in the opposite direction. This implies external controls on the sedimentary accommodation space, i.e. dynamic contributions. Even introducing unrealistic lithospheric effective elastic thicknesses (Te) of only 7.5 km does not produce a flexural response capable of matching the observed subsidence curves (Fig. 4).

We would expect dynamic signals to be important in the Maturin basin. It is near a very complex subduction scenario, where South America, Antilles and the Caribbean converge and overlap each other (Fig. 3). Jácome et al. (2003a), based on this geodynamic scenario, proposed that dynamic subsidence, driven by the associated mantle flows, might account for at least 45% of the residual basin depth deficit. These authors proposed that the South American Plate subducts subvertically underneath the Caribbean Plate as a continuation of the Lesser Antilles subduction zone, which plunges to the West at 30° along its main segment (cf. Russo et al., 1993). Based on seismic tomography of the upper mantle, Miller et al. (2009) and Miller and Becker (2012) suggested, instead, a lithospheric tear at the southeastern end of the South America-Caribbean plate boundary with dominant subduction from the Lesser Antilles to the West, and minor influence of the Caribbean to the East. In that scenario South American oceanic crust slightly subducts beneath the Antilles. Independently of these geometric controversies, and for the purpose of this review, it is clear that the Maturin basin has rested above a large amount of slab (mass

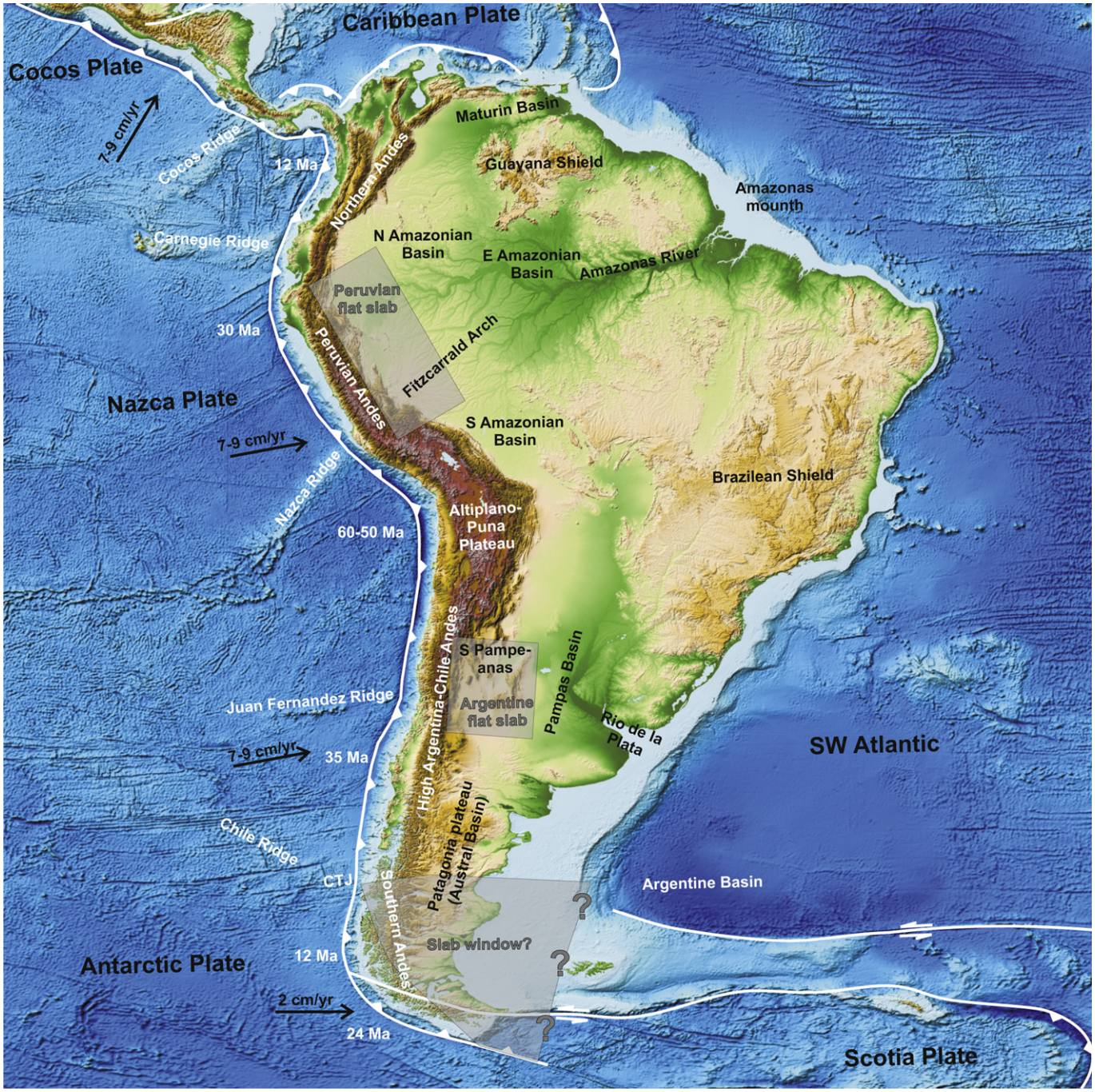

Fig. 3. Tectonic and geodynamic scenario of South America. Regions described in the text are shown for reference. Note the correlation of oceanic ridges, flat slab segments and the formation of inland topographies within the distal foreland (Fitzcarrald Arch and Sierras Pampeanas, in Peru and Argentina, respectively). The subduction of a triple junction and formation of a slab windows correlate, in turn, with the development of the Patagonia plateau. East of the Patagonia plateau is located the deep Argentine Basin.

anomaly) since the Miocene (Jácome et al., 2003b), when the complex subduction history of northern South America started. Given that the subduction is subvertical in both models, dynamic topography should focalize (according to the theory) over the plugging slab.

Jácome et al. (2003a) calculated dynamic topography in this segment using a finite element model and simple subduction geometry. The slab (South America in this case) was 50–100 km thick and extended in depth to ~200 km. The density contrasts were between 50 and 100 kg/m^3 with respect to the surrounding mantle (Fig. 4). The maximum dynamic topography wavelength was localized across the vertical subducting slab. The best fit between observations and modeling was obtained with a 50-km slab and the highest density contrast. The mantle convection forces associated with subduction reproduced ~2 km of subsidence (amplitude) across ~200 km (wavelength) (cf. Jácome et al., 2003a). When the tectonic loading and dynamic subsidence were combined the best fit to the observed subsidence curve required low Te (7.5 km). We speculate that alternatively increasing the viscosity or/and density contrast in the flow model might have a similar impact on the results. The Jácome et al. (2003a) results show short wavelengths of dynamic topography, similar to flexural wavelengths (<300 km). A

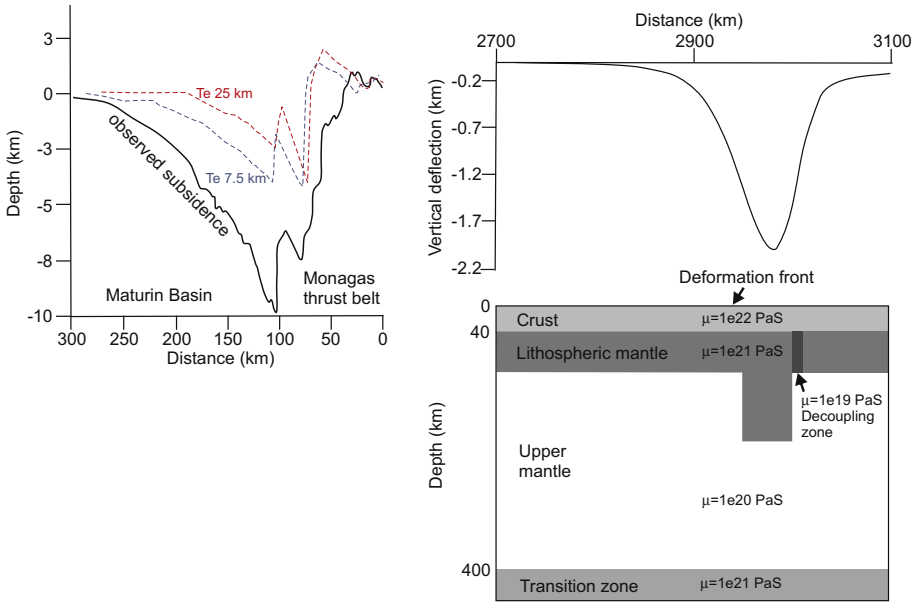

Fig. 4. Comparison between a flexural model and a predicted dynamic topography in the northernmost South America, Maturin Basin, eastern Venezuela (after Jácome et al., 2003a, b). The top left is a comparison between observed and modeled sediment-loaded subsidence using Te = 25 km and Te = 7 km. The graph to the top right shows the flow model result (dynamic topography) across eastern Venezuela. The bottom sketch illustrates the geometry and physical parameters used in modeling.

likely explanation of this wavelength overlapping might be their model design. This considered a thin and vertical slab, high viscous crust and decoupling zone within the lithospheric mantle. Billen and Gurnis (2001) also proposed narrow dynamic wavelengths (e.g., Tonga) in low-viscosity subduction wedge scenarios. This could be occurring in the Caribe as well.

5.2. The Amazonian foreland basins and Fitzcarrald Arch

The Andean Amazonian foreland basin spans ~2000 km along and across strike, between approximately 5° N to 12° S (Fig. 3), covering most of the northern South American countries, Venezuela, Colombia, Ecuador, Peru and Brazil. Espurt et al. (2007) defined it as an atypical foreland system (when compared with the classical DeCelles and Giles (1996) model), dissected along strike by the Fitzcarrald Arch. This W-E upwarping zone divides the foreland into two basins: (a) the Marañon-Ucayali-Acre basins to the north and (b) the Madre de Dios basin to the south (Räsänen et al., 1990; Mathalone and Montoya, 1995; Latrubese et al., 2010). The onset of synorogenic sedimentation is Paleogene (Campbell et al., 2001; Hermoza et al., 2005; Hoorn et al., 2010), and is associated with the first shortening events in the High Cordillera, but the thickest successions are younger (Miocene). Basin evolution can be divided in two major intervals, Paleogene and Miocene to present, separated by Ucayali unconformity (Campbell et al., 2001). This surface and two contrasting sequences correlate with the major tectonic change in deformation style in northern Peru (Hermoza et al., 2005) and the development of "Alpine landscapes" in the High Cordillera at ~12 Ma (cf. Hoorn et al., 2010). Further East, along the Atlantic margin, these changes were correlated with the formation of marine megafans at the Amazon River mouth and an increase in the sediment supply (Figueiredo et al., 2009). All these observations point to the Mio-Pliocene as a significant tectonic episode during the Amazonian basin configuration.

Although the Amazonian basin is likely one of the mega-foreland systems on Earth, no subsidence and flexural estimates are known. Furthermore, very few estimates of shortening have been published across the Peruvian Andes (Megard, 1984, 1987; Hermoza et al., 2005; Gotberg et al., 2010) to calculate the topographic loads used in a flexural analysis, therefore we estimate our own. From such studies one can estimate the deficits or excesses in the creation of sediment accommodation spaces. In the central Peruvian Andes the total orogenic shortening is ~30% (Megard, 1987), that is ~115 km from an orogenic width ~380 km). The 150-km wide Eastern Cordillera, the easternmost part of the orogen and youngest deformation belt, would have been shortened ~84 km in northern Peru (~40% Hermoza et al., 2005).

Based on the Hermoza et al. (2005) and Megard (1987) shortening reconstructions above, we compute (Fig. 5) a preliminary elastic flexural model to better understand the tectonic subsidence of Northern Amazonia that were compared then with stratigraphic thickness records (e.g., Espurt et al., 2007; Latrubesse et al., 2010). We used the Cardozo and Jordan (2001) numerical approach, an effective elastic thickness (Te) of 30–40 km (cf. Tassara et al., 2007) and other rheological parameters from Turcotte and Schubert (2002). Three load reconstructions were tested (Fig. 5), which represent the maximum and minimum boundaries: (1) a right-triangle load geometry geometrically distributed with base 80 km and height 10 km to the west that represents 40% of shortening (Hermoza et al., 2005), (2) a rectangle 380 km × 3 km that results from distributing the 115 km of shortening along a 380-km orogen (Megard, 1987), and (3) a localized load on the Eastern Cordillera (youngest deformation belt), represented by a rectangle of 170 km × 6 km, using Megard's (1987) shortening estimates. The results with loads (1) and (2) show a foredeep of ~1200 m depth extending for ~240 km from the easternmost thrust front to the forebulge. Model (3) generates a ~2500 m foredeep. Espurt et al. (2007) documented ~1000–1500 m of Cenozoic thicknesses (reflectors at ~1.2 s TWT tied to borehole data), matching the distributed load models. In the Acre sub-basin, approximately across 7° SL, but further East, Latrubesse et al. (2010) reported comparable strata thicknesses of ~1100 m. But this latter record is ~400 km away from the easternmost Andean load, where the flexural calculations amount to only a few meters. It is rather unlikely the Andean loads control the subsidence of this sub-basin as suggested by Latrubesse et al. (2010) given that, even using unreal large Te

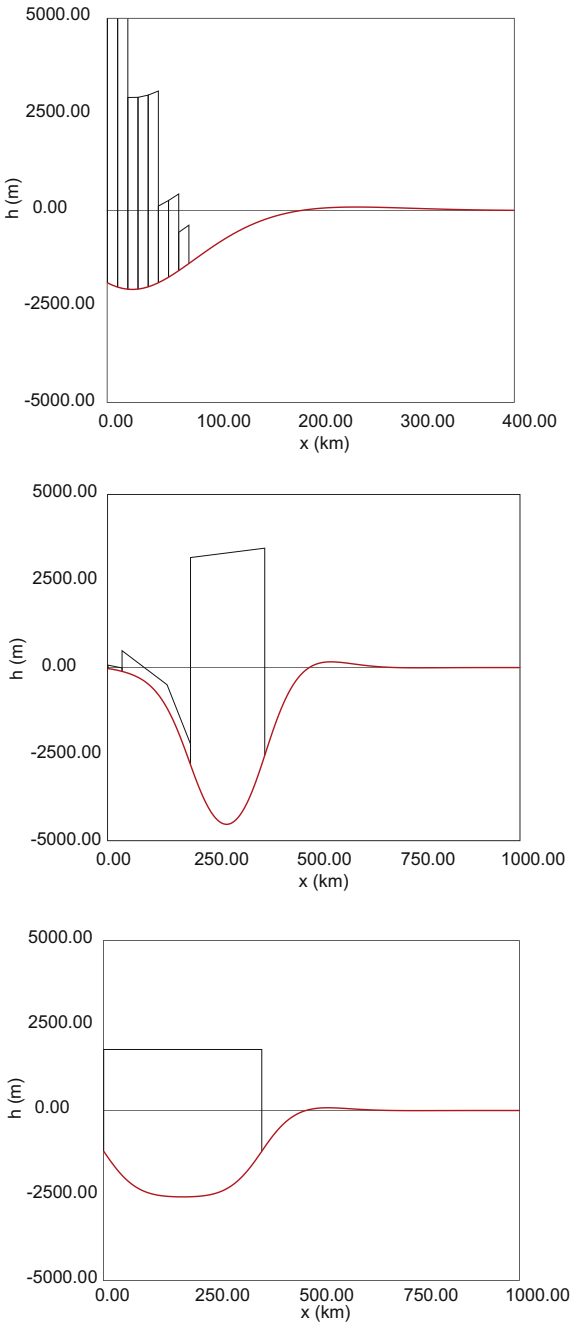

Fig. 5. Flexural models of the Peruvian Andes. The load reconstructions were based on the shortening estimations and balanced cross sections of Megard (1987) and Hermoza et al. (2005). The model to the top represents a wedged load, the center model a localized load in the frontal part of the thrust system and the bottom load is a even distributed load across the orogen. Note that the maximum depressions (foredeep) are <2.5 km deep and localized in <100 km across strike from the loads. Rheological parameters used in the calculations are described in the text.

values (>50 km), the maximum accommodations will still generate close to the load (<100 km).

Similar to that described earlier for Venezuela, overlapping mechanisms would seem to drive the Miocene-Pliocene subsidence in the Amazonian basins. While, the Eastern Cordillera loads would be large enough to accommodate sediments along the western depocenters, additional forces are required to the East, in central Amazonia (e.g., Acre sub-basin).

Martinod et al. (2008), Shephard et al. (2010) and Eakin et al. (2012) proposed that the subsidence and the subsequent Pliocene-Present uplift of the Amazonas landscape were strongly controlled by Nazca subduction dynamics. But none of these studies accounts for the effects of Andean mountain building to properly separate supra- and sub-lithospheric contributions. Martinod et al. (2008) suggested the <6 Ma morphology of the foreland after the major subsidence episode in the Miocene, was a result of the southward migration of the Nazca ridge (see also Espurt et al., 2007; Regards et al., 2009). Shephard et al. (2010) computed dynamic topography since the Eocene using an adjoint model to estimate the initial temperature structure from seismic tomography to reconstruct the slab geometry back in time, followed by a forward model of dynamic topography using the slab reconstruction (as in Liu and Gurnis, 2008). They proposed a >2000 m dynamic subsidence for the early Cenozoic (between 45 and 22 Ma) followed by positive changes in dynamic topography since the Miocene (Fig. 6). This positive change in dynamic topography was interpreted as the westward motion of South America over subducted slabs, which resulted in rebound of the western Amazonian region after 30 Ma, whereas the eastern basins continued subsiding. Although this might explain the development of depocenters like the Acre sub-basins (Latrubesse et al., 2010), the model failed in reproducing the northern and southern Amazonia. It is likely that Shepard et al. (2010)'s modeling was limited by the original seismic tomographic model they chose (both in spatial resolution and accuracy) and their assumptions about slab composition to adequately reproduce the complexity of slab morphology and structure and hence the dynamic topography in the Amazonian foreland. A recent preliminary study (Eakin et al., 2012) estimated the dynamic topography along the Peruvian foreland by creating a realistic flat-slab model using hypocentre locations. The calculation wavelengths matched rather well with the morphostructure of the Amazonian foreland described above, remarking the high incidence of the geometry and slab age in the dynamic signal.

5.3. The Bermejo-Pampas foreland of Argentina

In the south Central Andes between 27° and 34° SL, from Chile to central Argentina, there are three major morphotectonic features: (1) the Cordilleran belts (the Andes), (2) the highly-elevated Sierras Pampeanas broken foreland (a compressional basin and range system) and (3) the lowland Pampas plains (Fig. 3). Since the Early Miocene this segment has shortened orogenically by 40–100 km (Jordan et al., 1993). The tectonic and basin evolution across this segment has been strongly associated with the subduction dynamics of the Nazca plate (Jordan et al., 1983). The Miocene evolution was dominated by a normal-dipping slab, i.e., ~30° to the E, while the Pliocene to Present has been strongly controlled by flat subduction related to the collision of the Juan Fernandez ridge collision (Kay and Mpodozis, 2002).

The Miocene foreland, known as the Bermejo basin (cf. Jordan et al., 2001), was a typical prograding system that extended from the western Precordillera to the region where the broken foreland is today (Fig. 3). Jordan et al. (1993, 2001), Cardozo and Jordan (2001), and Dávila et al. (2007) summarized its tectono-stratigraphic evolution. The maximum sediment accumulations (>10 km) are recorded close to the Andean belts, in the foredeep, and only a few hundred meters have accumulated to the east, within the peripheral zones (Ezpeleta et al., 2006).

The modern foreland is >400 km eastward from the Miocene Bermejo basin and is known as the Pampean Plain or Pampas (Dávila et al., 2010) (Fig. 3). Underlying the modern Pampas foreland, a hundred meters of alluvial strata have been identified from seismic sections and boreholes (Marengo, 2006; Giménez et al., 2011). It is important to highlight that these Miocene units are not physically continuous (lateral progradation) with the Bermejo basin. It

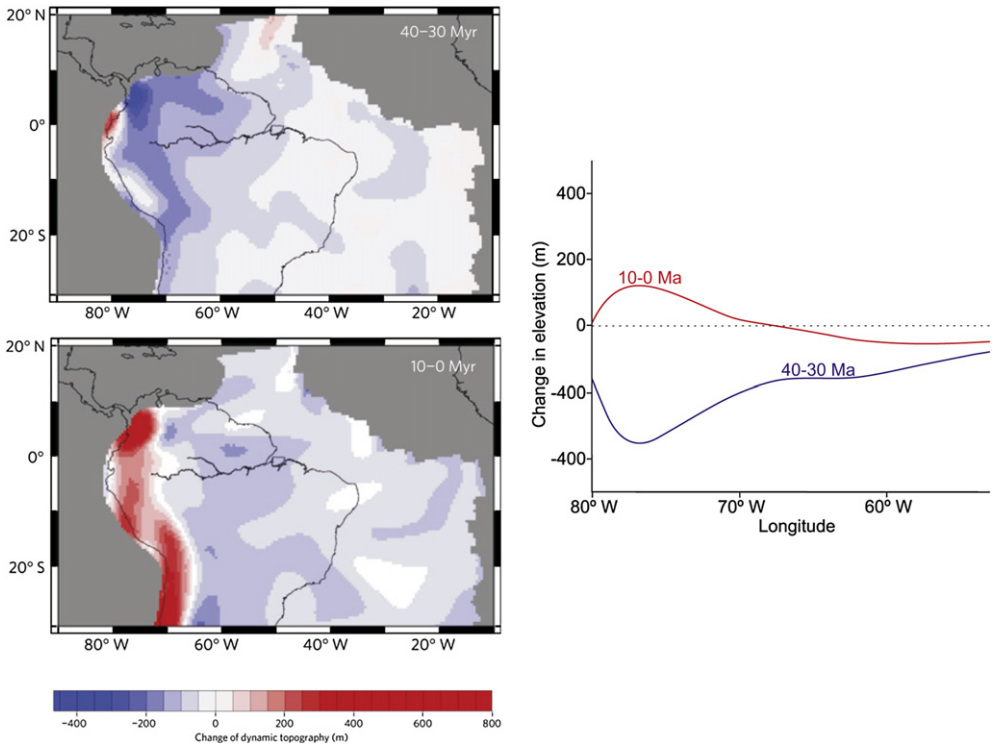

Fig. 6. Changes in dynamic topography in the northernmost South America (cf. Shephard et al., 2010). Note that the values tend to be positive from the Miocene across the Andean belt and negative along the distal plain. This model, however, did not reproduce the morphology of the Amazonian basins and Fitzcarrald Arch. See text for discussion.

represents, instead, a large and isolated sedimentary accumulation within the pericratonic foreland (Dávila et al., 2010), likely analogous to the sub-Acre depocenter in Brazil described above.

The accumulated shortening and the distribution of crustal roots do not explain the observed topographies along and across strike (Fromm et al., 2004; Dávila et al., 2005, 2010; Gilbert et al., 2006). As in Venezuela and Peru, the Miocene-Present topographies appear to have been strongly affected by dynamic forces (see also Dávila et al., 2007).

Cardozo and Jordan (2001) and Dávila et al. (2007) computed a flexural accommodation space, ~250 km in wavelength, with a maximum vertical amplitude of ~2 km and without any vertical subsidence toward the pericratonic areas (Fig. 8) between 20 and 9 Ma. Given that the recorded thicknesses (Fig. 7) in the foredeep are nearly 12 km (e.g., the Vinchina basin), it is clear that additional dynamic subsidence must have contributed to the creation of depositional spaces. Only an enormous amount of mass (e.g., excess of ~30 km × 100 km, equivalent to half Himalayan crust) could account for these thicknesses without dynamic topography. The missing 8–10 km of residual space in the foredeep obtained by subtracting the flexural amplitude from the observed subsidence as well as the accommodation space needed within the bulge areas, where there is no flexural subsidence (Fig. 7) is strong evidence of the dynamic contributions to topography. Dávila and Lithgow-Bertelloni (2011) quantified this non-isostatic subsidence by using the instantaneous flow formulation of Hager and O'Connell (1981). They proposed that the large subsidence of west-central Argentina was related to a normal dipping Nazca slab (no flat segments) during this time.

In the core of the Argentine foreland the Sierras Pampeanas broken foreland (Fig. 3) develops a long-wavelength upwarp during the Pliocene-Present period, associated with the arrival of the flat subduction (Strecker et al., 2009; Dávila et al., 2012). This slab flattening correlates with a clear volcanic shut-off, which persists to the present day (Kay and Gordillo, 1994). While the Sierras Pampeanas ranges are mostly the result of basement thrusting (Ramos et al., 2002), the extended and elevated intermontane basins located over 1 km above sea level require alternative explanations (see discussion in Dávila et al., 2012). In fact, geological information suggests a change from subsidence to uplift in the Pliocene (Dávila and Lithgow-Bertelloni, 2011). During the early Miocene the Sierras Pampeanas (like the rest of the Bermejo basin) subsided significantly (Dávila et al., 2007) followed, after flat subduction began, by uplift and exhumation of the Miocene basins. The ~100-m high flat mesas (Ezpeleta et al., 2006), consist of Miocene strata, are a clear evidence of this change.

The dynamic subsidence associated with the normal-dipping Miocene subduction history might also explain the accommodation of the Miocene sedimentary records in the subsurface Pampas as well as the Middle Miocene marine incursions within pericratonic areas (Paranaense flooding, Ruskin et al., 2011 and references therein). Although the broken foreland loading (e.g., the Sierras de Cordoba) close to the Pampas would be the most likely effect on the subsidence, Dávila et al. (2010) demonstrated that the isopach distribution (cf. Marengo, 2006; Dávila et al., 2010) cannot be reproduced by only thrust stacking (Fig. 10). They proposed dynamic subsidence to account for the space deficits. The effect of mantle dragging forces in the Pampas at the leading edge of the flat slab would have persisted until today, as evidenced by Quaternary stratigraphy and modern geomorphology (Dávila et al., 2010). It is important to notice that, in contrast to previous works in flat subduction settings (e.g., Burgess et al., 1997; Liu et al., 2008; among others), Dávila et al. (2010) proposed dynamic subsidence from the slab leading edge forward, i.e., eastward for the South American examples (and not across the entire flat slab as was previously suggested). In fact, we demonstrate below that flat-slab segments are more prone to positive changes in dynamic topography (i.e., relative uplift) than negative subsidence. (Fig. 9).

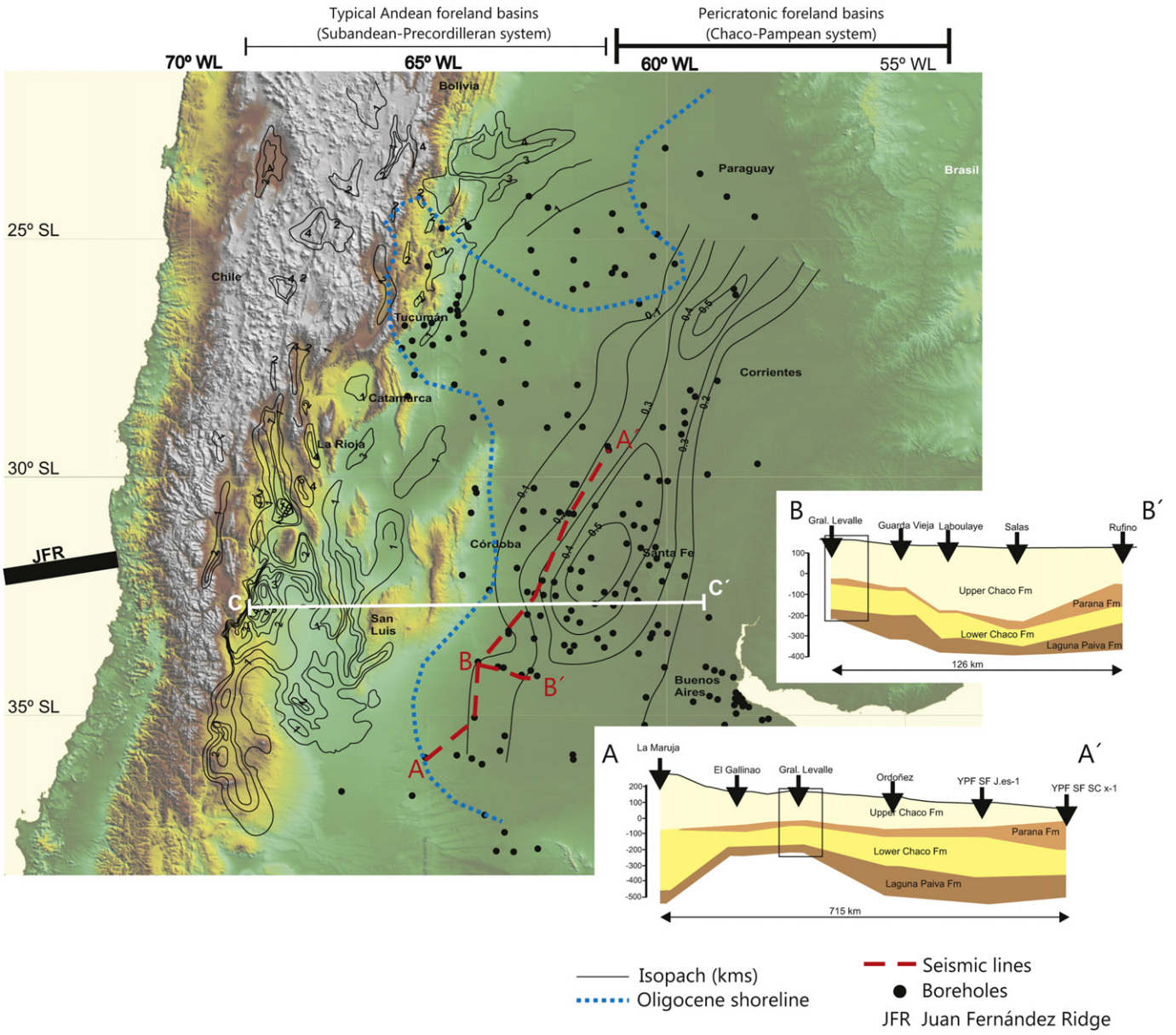

Fig. 7. Elevation model of the south Central Andes overlapped by the Neogene isopach map of the sedimentary basins of west-central Argentina. The cross sections (from seismic sections and boreholes, after Marengo, 2006; Giménez et al., 2011) show the Neogene-Present basin geometry beneath the Pampas plain. C–C′ shows the location of the total subsidence curve in Fig. 8. The location of the aseismic Juan Fernandez ridge is shown as reference.

6. The southern Patagonian foreland

The southern Patagonian foreland basins are located at the latitude of the present-day Chile Triple Junction (CTJ), where the Chile seismic ridge subducts beneath South America (Fig. 3). The CTJ migrated northward in the last 14 Ma, from 54° S to its present-day position at ~46° S (Breitsprecher and Thorkelsonet, 2009). Northward of the CTJ, the subduction of Nazca plate has been "normal" since the Miocene, in terms of dip angle and extent within the mantle, whereas to the south the Antarctic plate subduction has been negligible, only 100 km beneath South America (Breitsprecher and Thorkelson, 2009). This discrepancy led several authors to propose an asthenospheric slab window (Ramos and Kay, 1992; Kay et al., 1993; Gorring et al., 1997, 2003; Gorring and Kay, 2001; Breitsprecher and Thorkelson, 2009; Russo et al., 2010) (Fig. 11), which would have influenced the Late Miocene to present topography of Patagonia (Guillamé et al., 2009; Pedoja et al., 2011). Seismic studies (P-wave velocity tomography, Russo et al., 2010) support this interpretation, which show low velocities (hot mantle?) and no high velocities (slab) between 100 and 200 km (Fig. 13).

The south Patagonia geology consists of a low-elevation Cordilleran thrust belt (elevation under 3000 m above sea level, Ramos, 2005) and a typical foreland basin system, known as the Magallanes (Austral) Basin (see Biddle et al., 1986; Ramos, 1989; Ghiglione et al., 2010; among others) (Fig. 3). The main foreland sedimentation occurred at these latitudes between the latest Cretaceous and Early Miocene (Fosdick et al., 2011) and the uppermost foreland strata are ~14 Ma (Santa Cruz Fm., Blisniuk et al., 2005). After the Miocene sedimentation episode and the subduction of the CTJ, the south Patagonian foreland started to uplift (Blisniuk et al., 2005; Guillamé et al., 2009). A 6-my protracted unconformity (from 14 to 8 Ma) covered by the gravel sheets of the "Rodados Patagonicos" (<10 m thick, Parras et al., 2008) and the pervasive development of fluvial terraces (Guillamé et al., 2009) carving the

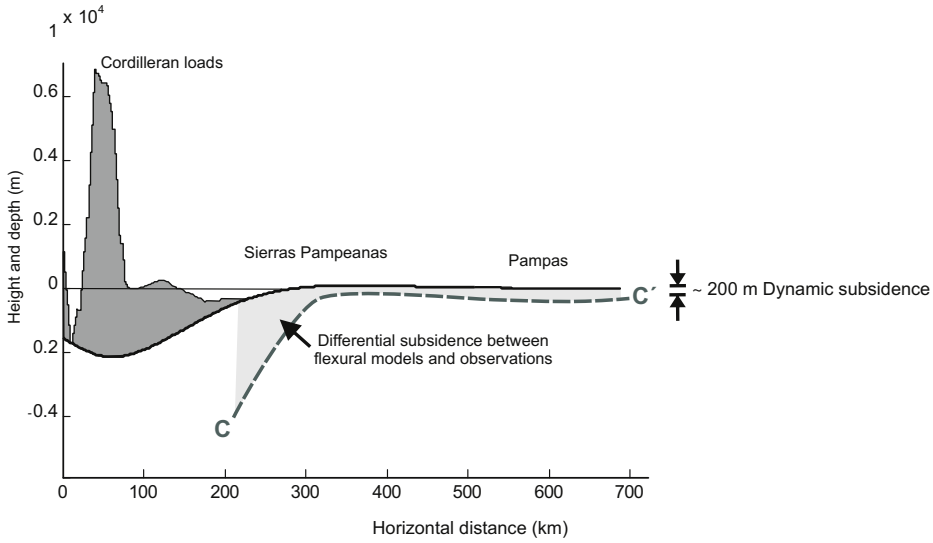

Fig. 8. Flexural model of the Bermejo Basin (after Davila et al., 2007). The dash line shows the measured subsidence curve (see location in Fig. 7, dash red lines A–A′ and B–B′) and the grey area (between the solid black and grey dash curves) represent the mismatching between the flexural model and stratigraphic observations. This indicates additional forces are required to account for the Neogene accumulations. In the forebulge and backbulge areas (from 300 km eastward), ~200 m of distal alluvial sediments might represent the records of a dynamic subsidence signal (see text and Dávila et al., 2007 for further discussions).

flat and elevated (>500 m above sea level) plateau support the inference of uplift. Extensive tholeiitic plateau lavas <12 Ma (Gorring et al., 1997) lay on the Patagonian plateau. Most of the basalts postdate the latest foreland sedimentation (i.e., ~14 Ma). They are not deformed and slightly tilted to the E (Lagabrielle et al., 2004). This implies that the main shortening would have ceased in south Patagonia at ~13 Ma, coeval with the plateau formation and northward migration of the seismic Chile ridge (Breitsprecher and Thorkelsonet, 2009).

The orogenic shortening in south Patagonia is between 45 and 22 km at ~48.5° SL (Ramos, 1989), which represent an accumulated deformation of ~10–20% (Fosdick et al., 2011). Flexural analyses (Fig. 12a) (Ghiglione et al., 2010) using lateral variations of Te across the foreland reproduced the depocenter positions and their lateral migration but the predicted amplitudes did not satisfy observed thickness of sediments in the foreland (Fig. 12b). Additional loads are required to accommodate the thick sedimentary sequence, locally greater than 8 km (Ramos, 1989).

Guillamé et al. (2009) suggested possible dynamic contributions in Patagonia (Fig. 14a). This model was based on a simple 3-D Newtonian Stokeslet flow approximation (Morgan, 1965; Batchelor, 1967; Harper, 1984; Husson, 2006), used a subduction-dipping angle of 37° to the E, a slab thickness of 50 km and density contrast between mantle and slab of 80 kg/m^3. This setting would represent the tectonic scenario prior to the subduction of the CTJ, with a "normal" subducting slab. The calculations reproduced an Oligocene-Middle Miocene dynamic subsidence of ~1 km (Guillamé et al., 2009) (Fig. 14a). But this is not sufficient to account for the ~8-km foredeep, even when adding the flexural calculations of Ghiglione et al. (2010) (Fig. 12). Future studies in Patagonia will assist us in reducing this large mismatching among observations and flexural-dynamic calculations.

The most significant change in the subduction dynamics in the southernmost South America occurred between the Late Miocene to Present. During this time and an incipient subduction regime developed under Southern Patagonia, where the Antarctica slab subducted for only 100 km (Breitsprecher and Thorkelsonet, 2009). Alongside the incipient subduction there was an upwelling cell driven by the subduction of the Chile ridge (Guillamé et al., 2009). The incipient slab would have generated little to no negative dynamic topography, while upwellings would generate positive dynamic topography.

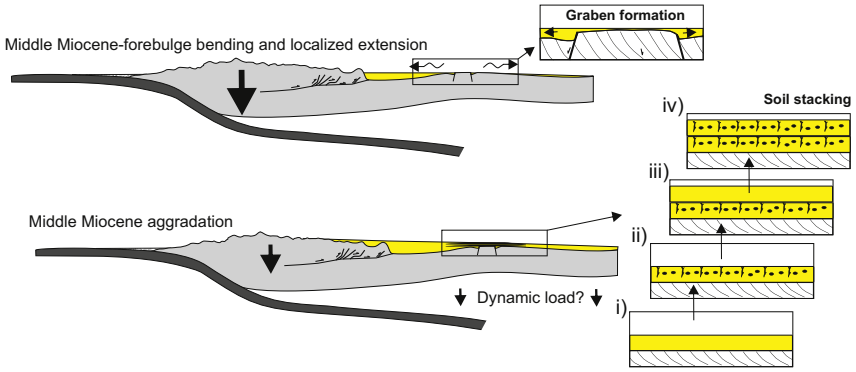

Fig. 9. Evolution of the Argentine foreland previous to the arrival of flat subduction in the south Central Andes of Argentina during the early-middle Miocene (after Dávila et al., 2007). Note the occurrence of distal alluvial facies (paleosoils) lapping the upwarping forebulge area, where normally no accumulations preserve. These deposits, together with the large mismatching between the flexural curve and total subsidence curve (see Fig. 8), suggest a regional and long-wavelength subsidence during the formation of the Bermejo Basin.

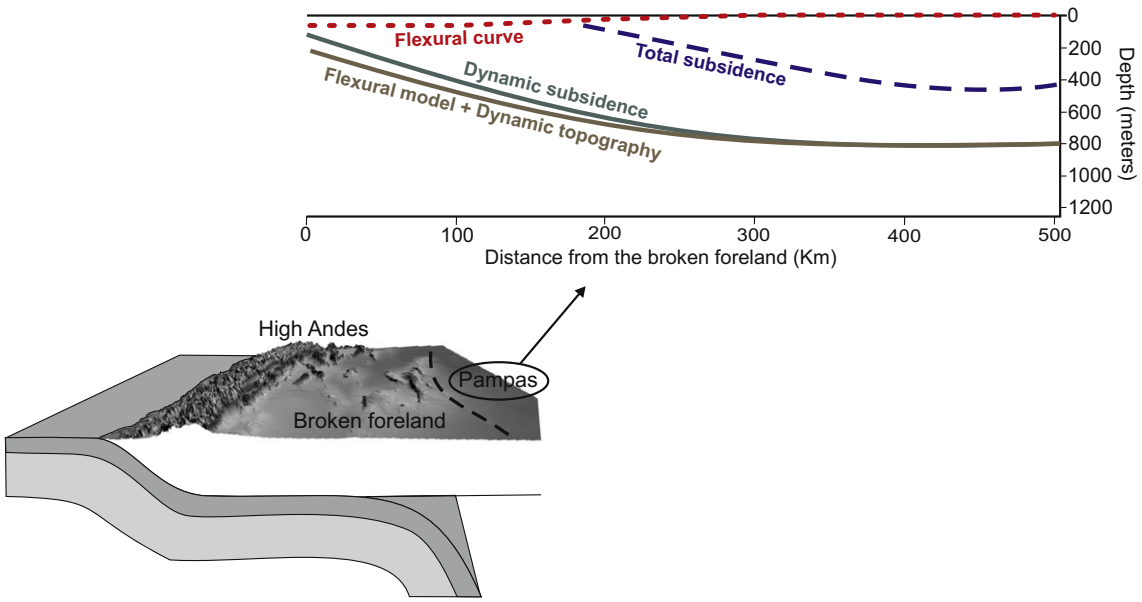

Fig. 10. Subsidence analysis in the Argentine Pampas (after Dávila et al., 2010). Total subsidence curve in blue, flexural model in red and dynamic topography in grey. The brown line represent the flexural curve plus dynamic topography. Note the flexural calculation in red cannot account for the observed sedimentary record (total subsidence in blue). Although dynamic topography explains the basin geometry in blue, it cannot reproduce the amplitudes (after Davila et al., 2010). The location of the Pampas, at >500 km from the high Andes, is shown for reference in the bottom sketch.

Guillamé et al. (2009) modeled the influence of the CTJ on Patagonian topography using the same approach detailed above. The dynamic response was quantified for four subducting ridge segments with lengths of 400, 200, 200, and 50 km that would correspond to four subduction episodes (13.5 Ma, 12 Ma, 6 Ma, and 3 Ma, respectively; Guillamé et al., 2009). The largest dynamic uplift (~800 m) was calculated close to each subducted ridge segment (Fig. 14b), whereas the estimated tilting was ~0.1%, to the east. This model matches fairly well with semi-quantitative morphometric analyses of the terrain (Guillamé et al., 2009). The better matching of the uplifting model compared with the subsidence model in Patagonia is because the amount of vertical displacement required to account observations is only a few hundreds of meters. The basin subsidence requires, instead, several kilometers. The same problem occurs in other deep basin systems, like Vinchina basin in western Argentina (see above).

Large plateaus commonly develop in regions of upwelling, such as the African superswell (Lithgow-Bertelloni and Silver, 1998; Gurnis et al., 2000). In Patagonia, geological inferences suggest uplift and exhumation (Rodados Patagonicos), plateau uplift and river incision. This uplift episode, as Pedoja et al. (2011) proposed using morphological and chronological analyses along coastal cliffs, would have reached the Atlantic margin. They documented an abrupt change in the paleo-shoreline uplift at approximately the CTJ latitudes. The length-scale >500 km is comparable to the Southern African plateau.

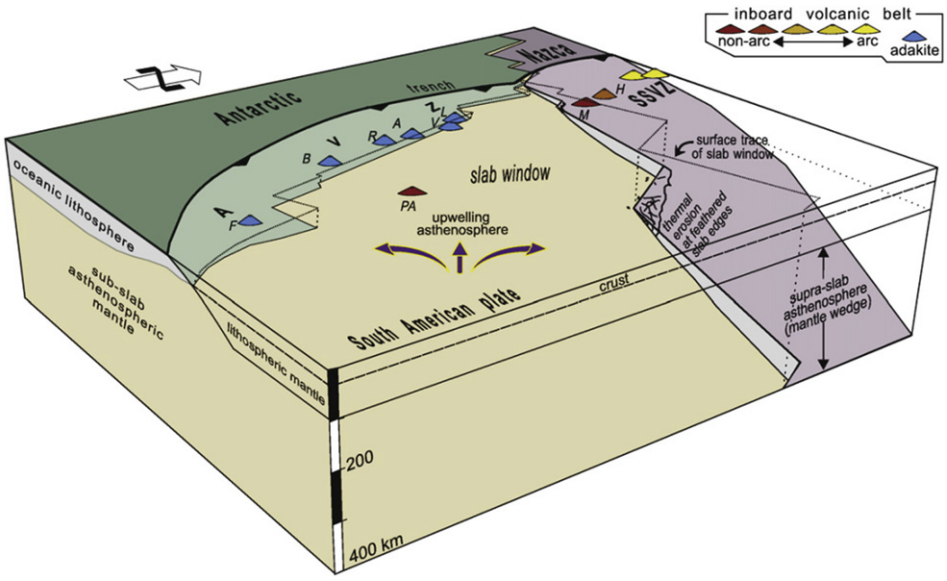

Fig. 11. Sketch of the Patagonian slab windows (after Breitsprecher and Thorkelson, 2009) associated to the subduction of the seismic Chile Ridge. Observe the slab geometry along Patagonia and with shallow depths (~100 km depth) in the Antarctic plate, to the South of the Chile triple junction, and normal in the Nazca plate, to the North. This geodynamic scenario is consistent not only with paleomagnetic reconstructions, but also with volcanic studies along Patagonia.

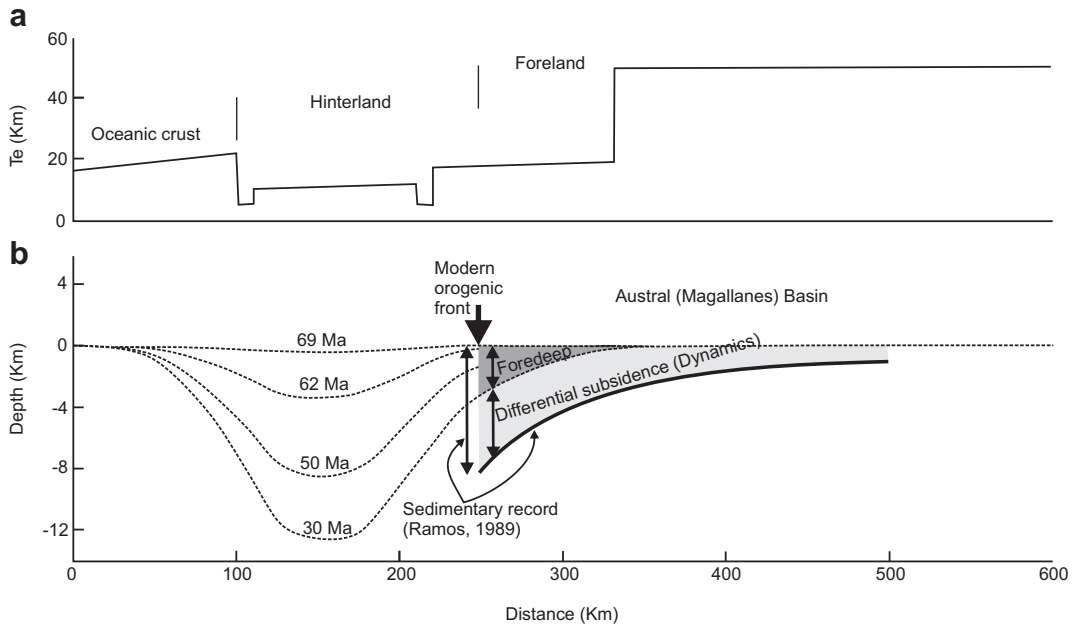

Fig. 12. Flexural models of the Austral (Magallanes) Basin (after Ghiglione et al., 2010) from the late Cretaceous to the Oligocene. The top graph shows the distribution from oceanic crust to the foreland of the Te used in the models. The bottom figure shows the sedimentary record of the basins (total subsidence, uncorrected by decompaction, after Ramos, 1989), the flexural curves (dash lines, after Ghiglione et al., 2010), and the location of the thrust front (leading edge of the tectonic load). The dark grey area depicts the foredeep location (deepest part of the foreland basin) and the light grey indicates the accumulations that could not be accounted by the models and might represent dynamic topography.

7. Argentine abyssal Basin

In the southwestern Atlantic, adjacent to the eastern continental margin of south Patagonia, we find one of the deepest oceanic depressions on Earth: the Argentine abyssal Basin (Fig. 3) or the "Hoya Argentina" (Nágera, 1927). This is a starved modern basin, with the oceanic floor >5 km below sea level. It holds at least ~3000 m of sediments (NGDC global sediment thickness grid, Divins, 2008). According to half-space cooling calculations (Hohertz and Carlson, 1998), improved recently by isostatically corrected age–depth variation studies (Winterbourne et al., 2009), the offshore hypsometry of the Argentine Basin is displaced ~1 km deeper with respect to

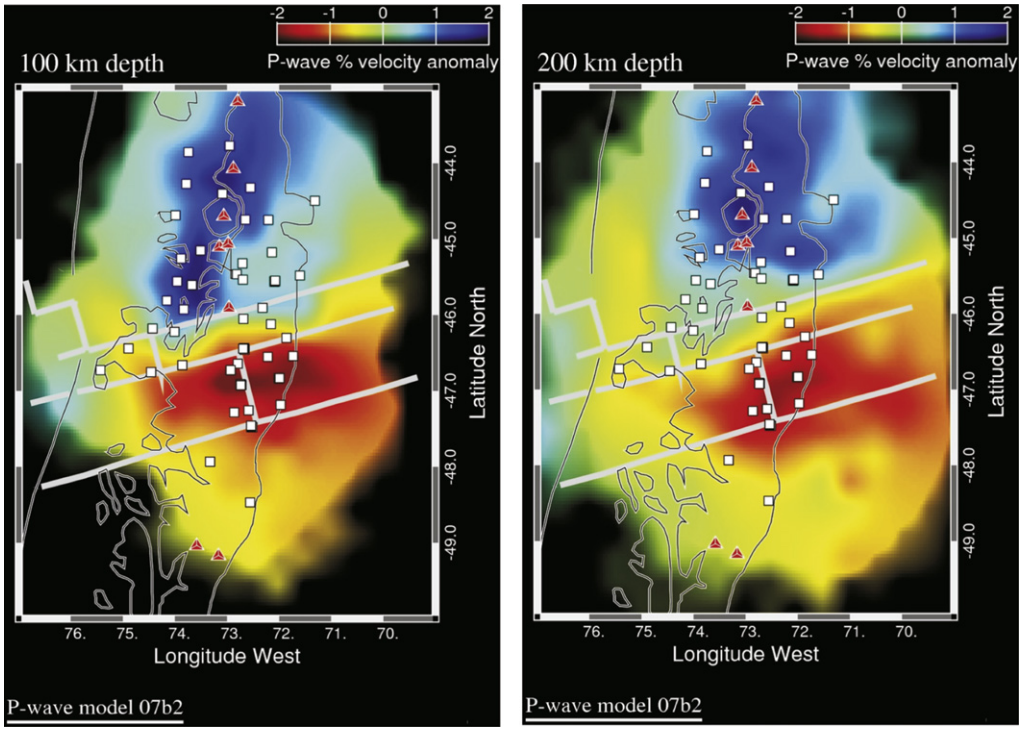

Fig. 13. P-wave velocity anomalies in southern Patagonia relative to radial Earth model IASP91, at 100 km (left) and 200 km (right) (from Russo et al., 2010). Note that the lowest velocity anomalies develop along the projection of the Chile Ridge (light grey lines) below the southernmost South America. Faster velocities (in blue), to the North, show the Nazca slab position.

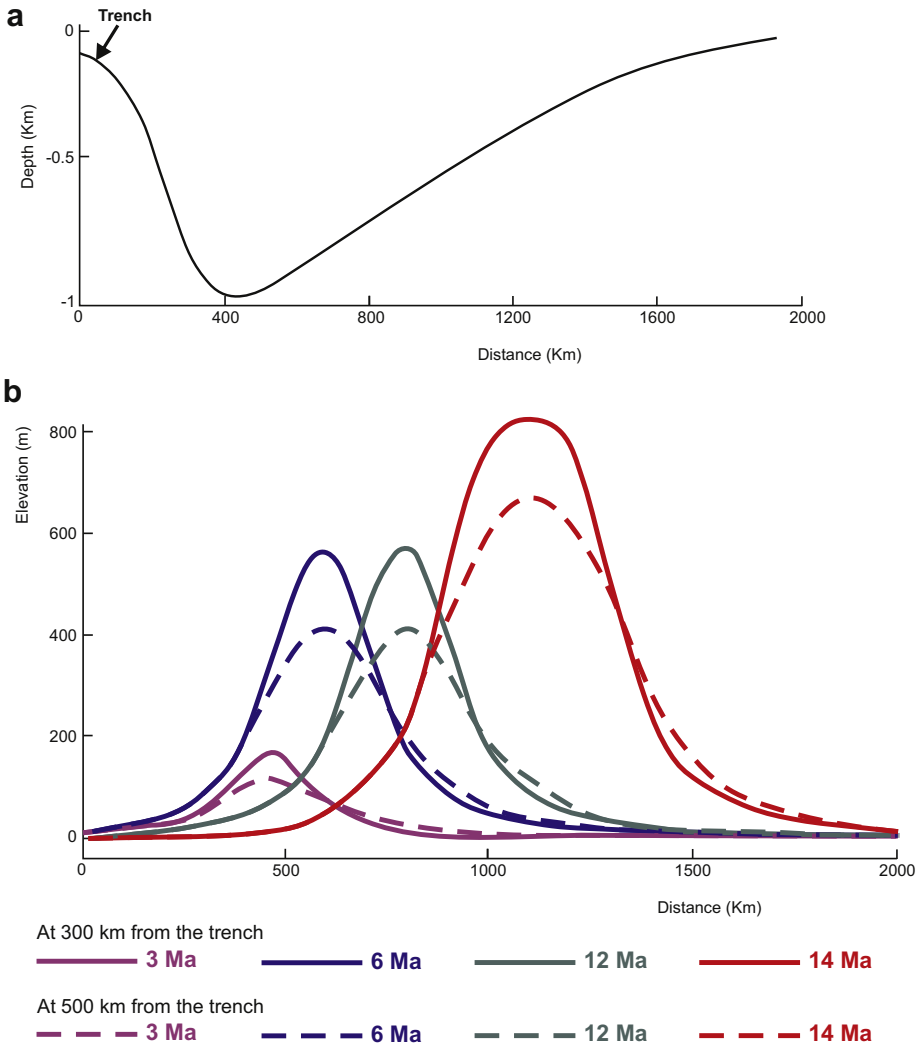

Fig. 14. **(a)** Dynamic subsidence and **(b)** uplift models of south Patagonia (from Guillaume et al., 2009). See text for further details. Note the maximum estimated dynamic subsidence is ~1 km and the maximum uplift ~0.8 km. The different lines and colors in b represent different topographic curves for 3, 6, 12 and 14 Ma and at 300 and 500 km from the trench.

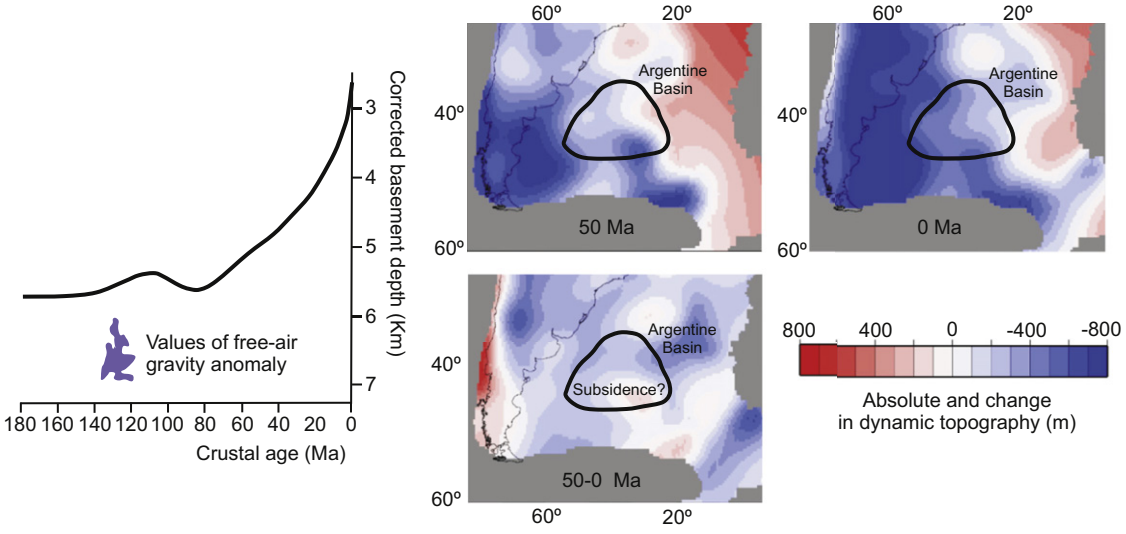

Fig. 15. Absolute dynamic topography at 50 Ma and 0 Ma in the SW Atlantic, across the Argentine Abyssal Basin (from Shephard et al., 2012) (top right). The bottom map shows the changes in dynamic topography from 50 to 0 Ma. The graph to the top left (after Winterbourne et al., 2009) compares the filtered free-air gravity anomalies in the SW Atlantic (blue polygon) and the calculated depth of the oceanic basement estimated from the half-space cooling calculations recently corrected isostatically (Winterbourne et al., 2009). Note the remarkable mismatching between curves, which suggests that additional mantle forces are required to account the gravity anomaly depth.

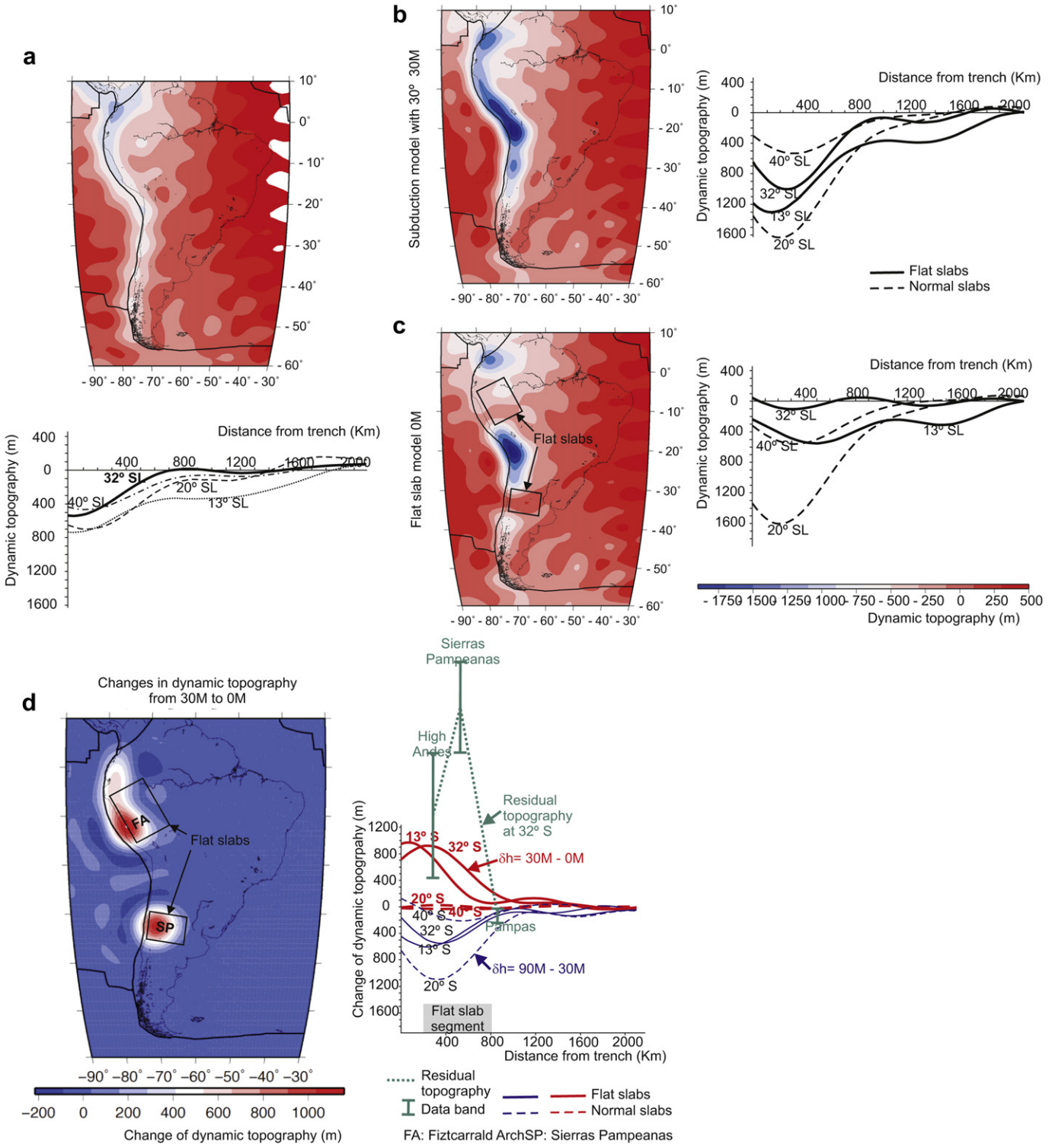

Fig. 16. Dynamic topography of South America using a slab-density instantaneous flow model (Hager and O'Connell, 1981). (a, b) Dynamic topography with a subvertical (90M, a, after Lithgow-Bertelloni and Richard, 1998) and 30° E (30M, b) subductions. (c) Results using the modern subduction geometry (Gutscher, 2002) with flat slabs (0M). The profiles were constructed for four transects, across two flat slab segments (13°and 32° SL) and two normal segments (20° and 40° SL). These models used a viscosity contrast that agrees with a low viscous asthenosphere (10-10^{-2}-1-50). (d) Change in dynamic topography from the 30M–0M models, i.e., from normal to flat subduction. The green line depicts the residual topography along three areas between the High Andes and the Pampas along 32° SL. Note the general trend matches remarkably well with the change in dynamic topography from normal to flat subduction, which is positive over the flat-slab regions and tends to negative across the pericratonic foreland. The data bars represent the minimum and maximum residual topography estimated from the minimum and maximum mean elevations.

global trends (Fig. 15). This depth difference coincides with a large negative free-air gravity anomaly (Winterbourne et al., 2009). Although upper mantle thermal cooling explains the general hypsometric trend, additional forces are required to account for the local kilometric deviations in amplitude below the basin. While Hohertz and Carlson (1998) related the mismatch to shallow asthenospheric flows, Steinberger (2007) and Winterbourne et al. (2009) proposed a negative dynamic support (dynamic subsidence), generated by convective circulation within the upper mantle. More recently, Shepard et al. (2012) associated this negative dynamic topography to the sinking slabs of the subducted Phoenix (Aluk) and Nazca plates since ~50 Ma. However, if this were the case, it would not explain latest Cenozoic uplift of Patagonia described above. Moreover, the present-day Nazca slab is not responsible for this depression as it generates dynamic topography westward of the deepest part of the Argentine basin (Dávila and Lithgow-Bertelloni, 2011).

There are other possible explanations. Subduction in the southern Andes is normal (i.e., Andean type) until the early Miocene, but a subduction gap or slab window develops after the subduction of the CTJ at ~14 Ma (Breitsprecher and Thorkelsonet, 2009; Russo et al., 2010). How large would the slab gap have been? Could it have affected the SW Atlantic sea floor? If the asthenospheric window projected further east, no negative dynamic topography support would be evident under the Argentine basin. Indeed the ridge reconstructions of Breitsprecher and Thorkelsonet (2009) and the seismic tomography of Russo et al. (2010) suggest the slab window (and mantle upwelling) extend to the Argentine abyssal Basin and hence we would expect mantle upwelling and positive dynamic topography rather than downwelling and negative dynamic topography. If that were the case, the corrected depths of the Argentine Basin should be deeper than reported after removing the hundred of meters of dynamic uplift along the Argentine coasts. This would require either deeper mantle structure (lower mantle?) or oceanic lithospheric delamination to explain the subsidence anomaly in the basin.

8. Latest dynamic topography results

We computed the dynamic topography over South America following the strategies explained in the last paragraph of the "*Computing Dynamic Topography*" chapter (see above). Our model solves the instantaneous viscous flow in the mantle induced by the presence of mass anomalies incorporated during the subduction history (Hager and O'Connel, 1981 formulation). We based the ancient slab reconstruction on geological approaches (e.g., Mpodozis and Ramos, 1989; Ramos, 2009) and the present-day scenarios on geophysical observations (see Dávila et al., 2010; Dávila and Lithgow-Bertelloni, 2011). The two geodynamic settings are: (i) A normal 30° − dip subduction constant along strike, from northern to southern Andes, which represents the early Miocene (Fig. 16a) and (ii) a modern scenario, with flat-slab segments and seismic ridge subduction (cf., Gutscher, 2002) that represents the Late Miocene to Today (Fig. 16b). For each setting the slabs extend to 700 km depth and are introduced into the mantle directly below the trench with a terminal velocity equal to the plate convergence rate, which decreases in the lower mantle by a factor proportional to the viscosity contrast between upper and lower mantle. (See Lithgow-Bertelloni and Richards, 1998 for further details). The slab density structure is a function of the age at the time of subduction (from Müller et al., 2008), except in flat segments where we assume the density contrast with respect to the mantle null to simulate net buoyancy. The latter is justified by the presence of thick crust in the subducted aseismic ridges, which is kinetically inhibited from transforming to eclogite. Cembrano et al. (2007) and Gans et al. (2011) also estimated close to zero density contrast across the Chilean-Argentine flat subduction zone, in agreement with our assumption. We find that subduction geometry and morphology control the pattern of dynamic topography, while the density structure of the slab determines its amplitude. To obtain the subsidence and uplift curves we subtracted the Miocene scenario from the present-day (Fig. 16c).

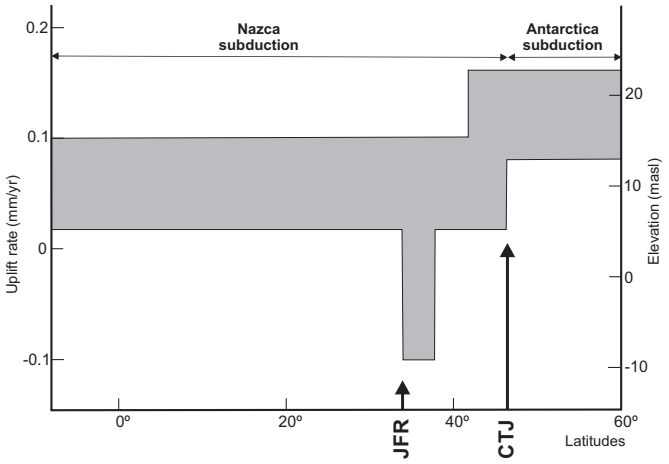

Fig. 17. Lateral variation in uplift rate and elevation along the east Atlantic coast of South America during the Quaternary (from Pedoja et al., 2011). Note the location of the Juan Fernandez Ridge (JFR) coincides with an anomalous subsidence area (in the Rio de la Plata). The Chile Ridge projection correlates with an abrupt positive step in coastal topography. These features suggest a clear connection between ridges and topography.

The results show a continental-scale subsidence belt along the Andean margin during the early Miocene. Although the dynamic subsidence amplitudes vary along strike consistent with the slab ages (density contrast) at the trench axis, clearly the Andean foreland system was supported by negative dynamic topography. Such support accounts for the residual sedimentary accommodation required matching the total subsidence observations with the flexural models (see above). With the along-strike segmentation of the subduction systems by flat slabs (Fig. 16b) (subduction of the Nazca, Juan Fernandez and Chile ridges) after the Miocene, the subsidence pattern and amplitude also changed. While the subsidence wave migrated and reduced greatly across flat-slab segments and cratonward, in areas with no flat segments it remains similar to the early Miocene. The changes in dynamic topography (Fig. 16d) are null in those segments that remain at "normal" dip angles and it is positive along flat slabs. These positive values, however, do not denote a positive contribution on the topography rather they imply positive vertical displacements with respect to the previous stage, because the dynamic negative support is reduced or eliminated. These results agree with geological observations along the flat-slab segments of Peru and Argentina, where the Plio-Holocene Fitzcarrald Arch and the high-elevation Sierras Pampeanas intermontane basins occur. Our model also explains the presence of the Quaternary Amazonian basins, in Peru and Brazil, and the Pampas of Argentina as basins that develop in response to the leading edge of the slab plunging back into the mantle. We dot not, however, predict the uplift of southern Patagonia because we do not account for the presence of a slab window or other possible active upwellings.

9. Discussion and conclusions

The Andes, from the high mountains to the foreland, have been considered as a typical example of an isostatically-compensated orogenic belt (see Watts, 2001). However, numerous measurements and observations, comparisons between seismic and gravity

Mohos (e.g., Fromm et al., 2004; Gilbert et al., 2006; Gans et al., 2011), as well as residual topography analyses (e.g., Steinberger, 2007), suggest the Cenozoic topographies cannot be supported only by the distribution of lithospheric loads, orogenic roots or antiroots and/or varying the density structure of the crust and lithospheric mantle. Additional forces are required. Although other mechanisms might contribute to the total topography (e.g., a better understanding of the lithospheric mantle contribution), the subduction-driven mantle convection forces are large enough to create the residual topography required to match observations (e.g., Gurnis et al., 2000).

The few dynamic topography studies from the northern to southern Andes indeed motivate further approaches in South America, not only for the variety of present-day tectonic settings but also for past geological events. In fact, the Altiplano-Puna plateau, the second largest plateau on Earth, has not been studied from this perspective, even when its anomalous low-relief elevation (Garzione et al., 2008) and associated subduction history (James and Sacks, 1999; Beck and Zandt, 2002) suggest a complex interaction between mantle dynamics, lithospheric detachment and final collapse (Capitanio et al., 2011). The proposed delamination (Kay and Mahlburg Kay, 1993) combined with slab steepening might result in a dynamic topography evolution not dissimilar from other areas of South America examined here. Recent laboratory experiments (e.g., Bajolet et al., 2012) have shown a topographic evolution from uplift, caused by upward mantle flow, followed by downwarping after the lithospheric removal. The result is intriguing because most previous studies on the Andean delamination focused on the most obvious and final effect, the plateau formation (cf. Barnes and Ehlers, 2009 and references therein), but no studies have paid close attention to the likely early depression generated during the collapse of the lower lithosphere. While the Early-Middle Miocene basins from Altiplano-Puna were interpreted as pre-delamination flexural depocenters (see Barnes and Ehlers, 2009 review and references therein), the new experiments (Bajolet et al., 2012) suggest not only that delamination could have started earlier but also that these basins, or at least part of their thicknesses, could be explained by delamination as well. It is important to remember that rebounding and uplifting (isostatic compensation and upwelling) as well as the extensive felsic volcanism (Kay and Mahlburg Kay, 1993) would have occurred after the subsidence episode.

There has been significant progress in mantle convection and subduction dynamics modeling (Tackley et al., 1993; Billen, 2008; Capitanio et al., 2011; among others), which has allowed for a more sophisticated analysis of the temporal changes in dynamic topography (e.g., Liu and Gurnis, 2008). However, there are still gaps to bridge, especially understanding the amplitude of dynamic topography, the shortest wavelengths at which it may act and the role of mantle and plate boundary rheology amongst others. Much work remains to be done in those areas and in achieving the resolution necessary to capture the complex morphology of slabs such as Nazca's. Much can be learned, however, by incorporating direct geological observations or different proxies (e.g., thermochronology, paleoaltimetry and morphometric analysis of the terrain) that can detect changes of surface elevation (see Garzione et al., 2008; Flowers, 2009; Hoke et al., 2009; Regard et al., 2009; Dávila et al., 2010; Flowers et al., 2011; Hartley et al., 2011; Dávila and Carter, 2013) rather than parameter exploration alone. A significantly better understanding of basin and orogenic belt dynamics, including their isostatic contributions would help in the computation of residual topography and provide strong constraints on mantle dynamics via dynamic topography. Such an understanding depends on better knowledge of lithospheric mantle and crustal structure. Unfortunately, very few geological studies have been orientated towards constrain dynamic topography amplitudes wavelengths and rates and they are largely driven by geodynamical modeling with some comparison to observations. However it is the combination of the geological proxies and geomorphic data with the dynamical models that there is the most power to understand the extent to which the interior controls the surface. Proxies, nevertheless, have limitations. While paleoelevation approaches have reported errors of approximately ±500 m, the most recent calculations of changes of dynamic topography, for example in Patagonia or northern Andes, are ~800 m (cf. Guillamé et al., 2009; Shepard et al., 2010). We think multiproxies analyses might represent a better alternative, combining and contrasting different sources of information with geological interpretations to reduce errors. Recently, for example, Dávila and Lithgow-Bertelloni (submitted) proposed a method to estimate the maximum dynamic topography amplitude using topographic swaths along stable landscapes, as the Argentine Pampas. According to this work, the maximum dynamic topography amplitude in such scenarios would be <300 m.

The Andes present many advantages with respect to other tectonic belts and make it an unrivaled natural laboratory to constrain dynamic topography and subduction dynamics. Complex processes affect the entire margin, from subduction of oceanic ridges to lithospheric delamination. It also shows exceptional geological features, which are still poorly explained and constrained. Regional surfaces, often interpreted as evidence of surface uplift, are abundant in the central Andes, and might represent mantle-driven epeirogenesis. One of these surfaces is the Pampean Peneplain (Jordan et al., 1989) in the Argentine foreland, affecting different rock ages and tectonic provinces. There are regional-scale low-relief surfaces along several Cordilleran locations: the Frontal Cordillera, Precordillera (Walcek and Hoke, 2012) and Puna-Eastern Cordillera. These regions are isostatically uncompensated (Gubbels et al., 1993; Gilbert et al., 2006) and might reflect mantle support.

Finally, and as a result of the large-scale lengths of the mantle driving forces (>300 km), the effects of dynamic topography might be detected and extracted in areas hundreds to thousands of kilometers away from subduction zones, across an entire continent (e.g., Spasojevic et al., 2008), so that the SW Atlantic passive margin of South America might record the effects of the Andean margin subduction as reported by Pedoja et al. (2011). They also associated the mismatch between local and global sea level curves along strike with the geodynamic setting, with subduction to the west and westward motion of South America from the east. But, although almost the entire Atlantic margin reflects uplift, Pedoja et al. (2011) suggested an anomalous sinking spot at the Rio de la Plata latitudes (Fig. 17), attributed to the sedimentation load and isostatic compensation. However, this is not observed at the latitudes of the mouth of the Amazon, where sedimentation rates would have been higher. We alternatively suggest that the flat slab of Argentina, located at this latitude, might be influencing this abnormal subsidence record. But, like in the rest of South America, more studies are required in order to better understand the dynamic topography of the continent.

Acknowledgments

We appreciate the comments of two anonymous reviewers and Editorial board that helped us to improve the original version of our manuscript. The 7th Framework Program, Marie Curie Actions (ERC), supports our ANDyN project (Andes-Nazca Experiment) in the Andes. We also appreciated funds and support by SECyT-UNC, CONICET, and FONCyT from Argentina and the University College London and NERC from the UK.

References

Bajolet, F., Galeano, J., Funiciello, F., Moroni, M., Negredo, A.-M., Faccenna, C., 2012. Continental delamination: insights from laboratory models.

Geochemistry Geophysics Geosystems 13, Q02009. http://dx.doi.org/10.1029/2011GC003896.
Barnes, J.B., Ehlers, T.A., 2009. End member models for Andean Plateau uplift. Earth-science Reviews 97, 117–144. http://dx.doi.org/10.1016/j.earscirev.08.003.
Batchelor, G., 1967. An Introduction to Fluid Mechanisms. Cambridge Univ. Press, Cambridge, U.K., p. 615.
Beck, S.L., Zandt, G., 2002. The nature of orogenic crust in the central Andes. Journal of Geophysical Research 107. http://dx.doi.org/10.1029/2000JB000124.
Biddle, K.T., Uliana, M.A., Mitchum, R.M., Fitzgerald, M.G., Wright, R.C., 1986. The stratigraphy and structural evolution of the central and eastern Magallanes Basin, southern South America. In: Allen, A., Homewood (Eds.), Foreland Basins. International Association of Sedimentologist Special Publication, vol. 8. Blackwell Scientific Publications, London, pp. 41–61.
Billen, M.I., 2008. Modeling the dynamics of subducting slabs. Annual Reviews of Earth and Planetary Science (Online access) 36, 325–356. http://dx.doi.org/10.1146/annurev.earth36.031207.124129.
Billen, M.I., Gurnis, M., 2001. A low viscosity wedge in subduction zones. Earth and Planetary Science Letters 193, 227–236.
Blisniuk, P.M., Stern, L.A., Chamberlain, C.P., Idleman, B., Zeitler, P.K., 2005. Climatic and ecologic changes during Miocene uplift in the Southern Patagonian Andes. Earth and Planetary Science Letters 230, 125–142.
Breitsprecher, K., Thorkelson, D.J., 2009. Neogene kinematic evolution of the Nazca–Antarctic–Phoenix slab windows beneath Patagonia and the Antarctic Peninsula. Tectonophysics 464, 10–20.
Burgess, P.M., Gurnis, M., Moresi, L.N., 1997. Formation of sequences in the cratonic interior of North America by interaction between mantle, eustatic, and stratigraphic processes. GSA Bulletin 108 (12), 1515–1535.
Campbell, K.E., Heizler, M., Frailey, C.D., Romero-Pittman, L., Prothero, D.R., 2001. Upper Cenozoic chronostratigraphy of the southwestern Amazon Basin. Geology 29, 595–598.
Capitanio, F., Faccenna, C., Zlotnik, S., Stegman, D., 2011. Subduction dynamics and the origin of Andean orogeny and the Bolivian orocline. Nature [P] 480 (7375), 83–86. Nature Publishing Group, England.
Cardozo, N., Jordan, T.E., 2001. Causes of spatially variable tectonic subsidence in the Miocene Bermejo foreland basin, Argentina. Basin Research 13, 335–357.
Cazenave, A., Thoraval, C., 1994. Mantle dynamics constrained by degree 6 surface topography, seismic tomography and geoid: Inference on the origin of the South Pacific Superswell. Earth and Planetary Science Letters 122, 219–297.
Cembrano, J., Lavenu, A., Yañez (coordinators), G., Riquelme, R., Garcia, M., González, G., Herail, G., 2007. Neotectonics. In: Moreno, T., Gibbons, W. (Eds.), The Geology of Chile. The Geological Society, London, pp. 147–178.
Chevalier, Y., González, G., Mata, S., Santiago, N., Spano, F., 1995. Estratigrafía Secuencial del Transecto El Pilar – Cerro Negro, Cuenca Oriental de Venezuela. In: VI Congreso Colombiano del Petróleo, Memorias, pp. 115–125.
Conrad, C.P., Husson, L., 2009. Influence of dynamic topography on sea level and its rate of change. Lithosphere 1, 110–120. http://dx.doi.org/10.1130/L32.1.
Conrad, C.P., Lithgow-Bertelloni, C., Louden, K.E., 2004. Iceland, the Farallon slab, and dynamic topography of the North Atlantic. Geology 32 (3), 177–180. http://dx.doi.org/10.1130/G20137.1.
Cross, T.A., Pilger Jr., R.H., 1978. Tectonic controls of late Cretaceous sedimentation, western interior, USA. Nature 274, 653–657.
Daradich, A., Mitrovica, J.X., Pysklywec, R.N., Willett, S.D., Forte, A.M., 2003. Mantle flow, dynamic topography, and rift-flank uplift of Arabia. Geology 31, 901–904.
Dávila, F.M., 2003. Transecta estratigráfica-estructural a los 28°30'–28°54' de Latitud Sur, sierra de Famatina, provincia de La Rioja, República Argentina. Tesis Doctoral Inédita, Facultad de Ciencias Exactas, Físicas y Naturales, Universidad Nacional de Córdoba (inédita), p. 516.
Dávila, F.M., Lithgow-Bertelloni, C., 2011. Dynamic Topography during Flat Subduction: Subsidence or Uplift?. American Geophysical Union Annual Meeting, San Francisco, USA.
Dávila, F.M., Carter, A. Exhumation history of the Andean broken foreland revisited. Geology, in press.
Dávila, F.M., Astini, R.A., Jordan, T.E., 2005. Cargas subcorticales en el antepaís andino y la planicie pampeana: Evidencias estratigráficas, topográficas y geofísicas. Revista de la Asociación Geológica Argentina 60, 775–786.
Dávila, F.M., Astini, R.A., Jordan, T.E., Gehrels, G., Ezpeleta, M., 2007. Miocene forebulge development previous to the broken foreland partitioning in the southern Central Andes, west-central Argentina. Tectonics 26, TC5016. http://dx.doi.org/10.1029/2007TC002118.
Dávila, F.M., Lithgow-Bertelloni, C., Giménez, M., 2010. Tectonic and dynamic controls on the topography and subsidence of the Argentine Pampas: the role of the flat slab. EPSL 295, 187–194.
Dávila, F.M., Giménez, M., Nóbile, J., Martínez, P., 2012. The evolution of the high-elevated depocenters of the northern Sierras Pampeanas (~28° SL), Argentine broken foreland, south-Central Andes: the Pipanaco Basin. Basin Research. http://dx.doi.org/10.1111/j.1365-2117.2011.00539.x.
DeCelles, P.G., Giles, K.A., 1996. Foreland basin systems. Basin Research 8, 105–123.
Divins, D.L., 2008. NGDC Total Sediment Thickness of the World's Oceans & Marginal Seas. http://www.ngdc.noaa.gov/mgg/sedthick/sedthick.html.
Eakin, C.M., Lithgow-Bertelloni, C., Dávila, F.M., 2012. Influence of Peruvian Flat-subduction Dynamics on the Evolution of the Amazon Basin. American Geophysical Union Annual Meeting, San Francisco, USA.
Espurt, N., Baby, P., Brusset, S., Roddaz, M., Hermoza, W., Regard, V., Antoine, P.-O., Salas-Gismondi, R., Bolaños, R., 2007. How does the Nazca Ridge subduction influence the modern Amazonian foreland basin? Geology 35, 515–518.
Ezpeleta, M., Davila, F.M., Astini, R.A., 2006. Estratigrafía y paleoambientes de la Formación Los Llanos (La Rioja, Argentina): Una secuencia condensada miocena en el antepaís fragmentado andino central. Revista de la Asociación Geolíogica Argentina 61, 171–186.
Figueiredo, J.J.P., Hoorn, C., van der Vem, P.H., Soares, E.F., 2009. Late Miocene onset of the Amazon River and the Amazon deep-sea fan: evidence from the Foz do Amazonas Basin. Geology 37, 619–622. http://dx.doi.org/10.1130/G25567A.1.
Flowers, R.M., 2009. Exploiting radiation damage control on apatite (U-Th)/He dates in cratonic regions. Earth and Planetary Science Letters 277, 148–155. http://dx.doi.org/10.1016/j.epsl.2008.10.005.
Flowers, R.M., Ault, A.K., Kelley, S.A., Zhang, N., Zhong, S., 2011. Testing mantle dynamic models from thermochronology constraints on the rise and fall of continental interiors. In: Proceeding Abstract, "Dynamic Topography Conference". The Geological Society of London, London, UK, p. 12.
Fosdick, J.C., Romans, B.W., Fildani, A., Bernhardt, A., Calderón, M., Graham, S.A., 2011. Kinematic evolution of the Patagonian retroarc fold-and-thrust belt and Magallanes foreland basin, Chile and Argentina, 51°30'S. Geological Society of America Bulletin 123, 1679–1698.
Fromm, R., Zandt, G., Beck, S.L., 2004. Crustal thickness beneath the Andes and Sierras Pampeanas at 30°S inferred from Pn apparent phase velocities. Geophysical Research Letters 31, L06625. http://dx.doi.org/10.1029/2003GL019231.
Gans, C., Beck, S., Zandt, G., Gilbert, H., Alvarado, P., 2011. Continental and oceanic crustal structure of the Pampean flat slab region, western Argentina, using receiver function analysis: new high-resolution results. Geophysical Journal International 186, 45–58.
García Castellanos, D., Fernandez, M., Torne, m., 1997. Numerical modeling of foreland basin formation: a program relating thrusting, flexure, sediment geometry and lithosphere rheology. Computer and Geosciences 23 (9), 993–1003.
Garzione, C.N., Hoke, G.D., Libarkin, J.C., Withers, S., MacFadden, B., Eiler, J., Ghosh, P., Mulch, A., 2008. Rise of the Andes. Science 320, 1304. http://dx.doi.org/10.1126/science.1148615.
Ghiglione, M.C., Quinteros, J., Yagupsky, D., Bonillo-Martínez, P., Hlebszevtich, J., Ramos, V.A., Vergani, G., Figueroa, D., Quesada, S., y Zapata, T., 2010. Structure and tectonic history of the foreland basins of southernmost South America. Journal of South American Earth Sciences 29 (2), 262–277.
Gilbert, H., Beck, S., Zandt, G., 2006. Lithospheric and upper mantle structure of central Chile and Argentina. Geophysical Journal International 165, 383–398.
Giménez, M., Dávila, F.M., Astini, R.A., Martinez, P., 2011. Interpretación gravimétrica y estructura cortical en la cuenca de General Levalle, Provincia de Córdoba, Argentina. Revista Mexicana de Ciencias Geológicas 28 (1), 105–117.
Gorring, M.L., y Kay, S.M., 2001. Mantle processes and sources of Neogene slab-window magmas in southern Patagonia. Journal of Petrology 42 (6), 1067–1094.
Gorring, M., Kay, S., Zeitler, P., Ramos, V., Rubiolo, D., Fernandez, M., Panza, J., 1997. Neogene Patagonian plateau lavas: continental magmas associated with ridge collision at the Chile Triple Junction. Tectonics 16 (1), 1–17.
Gorring, M., Singer, B., Gowers, J., Kay, S., 2003. Plio-Pleistocene basalts from the Meseta del Lago Buenos Aires, Argentina: evidence for asthenosphere-lithosphere interactions during slab window magmatism. Chemical Geology 193, 215–235.
Gotberg, N., McQuarrie, N., Carlotto Caillaux, V., 2010. Comparison of crustal thickening budget and shortening estimates in southern Peru (12–14°S): Implications for mass balance and rotations in the "Bolivian orocline". GSA Bulletin 122, 727–742.
Gubbels, T.L., Isacks, B.L., Farrar, E., 1993. High-level surfaces, plateau uplift, and foreland development, Bolivian central Andes. Geology 21, 695–698.
Guillaume, B., Martinod, J., Husson, L., Roddaz, M., Riquelme, R., 2009. Neogene uplift of central eastern Patagonia: dynamic response to active spreading ridge subduction? Tectonics 28, TC2009. http://dx.doi.org/10.1029/2008TC002324.
Gurnis, M., 1990. Ridge spreading, subduction, and sea level fluctuations. Science 250, 970–972.
Gurnis, M., Mitrovica, J.X., Ritsema, J., van Heijst, H.-J., 2000. Constraining mantle density structure using geological evidence of surface uplift rates: the case of the African superplume. Geochemistry, Geophysics, Geosystems 1. Paper number 1999GC000035.
Gutscher, M.-A., 2002. Andean subduction styles and their effect on thermal structure and interplate coupling. Journal of South American Earth Sciences 15, 3–10.
Hager, B.H., O'Connell, R.J., 1981. A simple model of plate dynamics and mantle convection. Journal Geophysical Research 86, 4843–4867.
Hager, B.H., Clayton, R.W., Richards, M.A., Dziewonski, A.M., Comer, R.P., 1985. Lower mantle heterogeneity, dynamic topography, and the geoid. Nature 313, 541–545.
Han, L., Gurnis, M., 1999. How valid are dynamic models of subduction and convection when plate motions are prescribed? Physics of Earth and Planetary Interiors 110, 235–246.
Harper, J.F., 1984. Mantle flow due to internal vertical forces. Physics of Earth and Planetary Interiors 36, 285–290. http://dx.doi.org/10.1016/0031-9201(84)90052-9.
Harrison, C.G.A., Miskell, K.J., Brass, G.W., Saltzman, E.S., Sloan II, J.L., 1983. Continental hypsography. Tectonics 2, 357–377.
Hartley, R.A., Roberts, G., White, N.J., Richardson, C.N., 2011. Transient convective uplift of an ancient buried landscape. Nature Geoscience. ISSN: 1752-0894 4. ISSN: 1752-0894, 562–565. EISSN:1752-0908.

Heine, C., Müller, R.D., Steinberger, B., Torsvikb, T.H., 2008. Subsidence in intracontinental basins due to dynamic topography. Physics of the Earth and Planetary Interiors 171, 252–264.
Hermoza, W., Brusset, S., Baby, P., Gil, W., Roddaz, M., Guerrero, N., Bolaños, R., 2005. The Huallaga foreland basin evolution: thrust propagation in a deltaic environment, northern Peruvian Andes. Journal of South American Earth Sciences 19, 21–34.
Hohertz, W.L., Carlson, R.L., 1998. An independent test of thermal subsidence and asthenosphere flow beneath the Argentine Basin. Earth and Planetary Science Letters 161, 73–83.
Hoke, G.D., Garzione, C.N., Araneo, D.C., Latorre, C., Strecker, M.R., Williams, K.J., 2009. The stable isotope altimeter: do Quaternary pedogenic carbonates predict modern elevations? Geology 37, 1015–1018.
Hoorn, C., Wesselingh, F.P., ter Steege, H., Bermudez, M.A., Mora, A., Sevink, J., Sanmartín, I., Sanchez-Meseguer, A., Anderson, C.L., Figueiredo, J., Jaramillo, C., Riff, D., Negri, F.R., Hooghiemstra, H., Lundberg, J., Stadler, T., Sarkinen, T., Antonelli, A., 2010. Amazonia through time: Andean uplift, climate change, landscape evolution and biodiversity. Science 330, 927–931.
Hung, E., 1997. Foredeep and thrust belt interpretation of the Maturin sub-basin, Eastern Venezuela Basin. Rice University, Houston, Texas, Unpublished MA thesis, p. 125.
Husson, L., 2006. Dynamic topography above retreating subduction zones. Geology 34 (9), 741–744. http://dx.doi.org/10.1130/G22436.1.
Jácome, M.I., Kusznir, N., Audemard, F., Flint, S., 2003a. The formation of the Maturín foreland basin, eastern Venezuela: thrust sheet loading or subduction dynamic topography. Tectonics 22 (5), 1–17.
Jácome, M.I., Kusznir, N., Audemard, F., Flint, S., 2003b. Tectono-stratigraphic evolution of the Maturin foreland basin: eastern Venezuela. In: Bartolini, C., Buffler, R., Blickwede, J. (Eds.), The Circum-gulf of Mexico and the Caribbean: Hydrocarbon Habitats, Basin Formation and Plate Tectonics. AAPG Memoir, vol. 79, pp. 735–749.
James, D.E., Sacks, I.S., 1999. Cenozoic formation of the Central Andes: a geophysical perspective. SEPM Special Publication. In: Skinner, B.J. (Ed.), Geology and Ore Deposits of the Central Andes, pp. 1–25.
Jordan, T.E., Zeitler, P., Ramos, V.A., Gleadow, A.J.W., 1989. Thermochronometric data on the development of the basement peneplain in the Sierras Pampeanas, Argentina. Journal of South American Earth Sciences 2, 207–222.
Jordan, T.E., Isacks, B.I., Allmendinger, R.W., Brewer, J.A., Ramos, V.A., Ando, C.J., 1983. Andean tectonics related to geometry of subducted Nazca plate. Geological Society of America Bulletin 94, 341–361.
Jordan, T.E., Allmendinger, R.W., Damanti, J.F., Drake, R.E., 1993. Chronology of motion in a complete thrust belt: the Precordillera, 30°–31°, Andes mountains. The Journal of Geology 101, 135–156.
Jordan, T.E., Schlunegger, F., Cardozo, N., 2001. Unsteady and spatially variable evolution of the Neogene Andean Bermejo Foreland Basin, Argentina. Journal of South American Earth Sciences 14, 775–798.
Kay, S.M., Gordillo, C.E., 1994. Pocho volcanic rocks and the melting of depleted continental lithosphere above a shallowly dipping subduction zone in the Central Andes. Contributions to Mineralogy and Petrology 117, 25–44.
Kay, R.W., Mahlburg Kay, S., 1993. Delamination and delamination magmatism. Tectonophysics 219, 177–189.
Kay, S.M., Mpodozis, C., 2002. Magmatism as a probe to the Neogene shallowing of the Nazca plate beneath the modern Chilean flat-slab. Journal of South American Earth Sciences 15, 39–57.
Kay, S.M., Ramos, V.A., y Márquez, M., 1993. Dominant slab-melt component in Cerro Pampa adakitic lavas erupted prior to the collision of the Chile rise in Southern Patagonia. Journal of Geology 101, 703–714.
Lagabrielle, Y., Suárez, M., Rossello, E.A., Hérail, G., Martinod, J., Régnier, M., De la Cruz, R., 2004. Neogene to Quaternary evolution of the Patagonian Andes at the latitude of the Chile Triple Junction. Tectonophysics 385, 211–241. http://dx.doi.org/10.1016/j.tecto.2004.04.023.
Latrubesse, E.M., Cozzuol, M., da Silva-Caminha, S.A.F., Rigsby, C.A., Absy, M.L., Jaramillo, C., 2010. The Late Miocene paleogeography of the Amazon Basin and the evolution of the Amazon River system. Earth-Science Reviews 99, 99–124.
Lithgow-Bertelloni, C., Gurnis, M., 1997. Cenozoic subsidence and uplift of continents from time-varying dynamic topography. Geology 25 (8), 735–738.
Lithgow-Bertelloni, C., Richards, M.A., 1998. The dynamic of Mesozoic and Cenozoic plate motion. Reviews of Geophysics 36, 27–78.
Lithgow-Bertelloni, C., Silver, P.G., 1998. Dynamic topography, plate driving forces and the African superswell. Nature 395 (6699), 269–272.
Lithgow-Bertelloni, C., Guynn, J.H., 2004. Origin of the lithospheric stress field. J. Geophys. Res. 109 (B1). http://dx.doi.org/10.1029/2003JB002467. Article B01408.
Liu, L., Gurnis, M., 2008. Simultaneous inversion of mantle properties and initial conditions using an adjoint of mantle convection. Journal of Geophysical Research 113, B08405. http://dx.doi.org/10.1029/2008JB005594.
Liu, L., Spasojević, S., Gurnis, M., 2008. Reconstructing Farallon plate subduction beneath North America back to the Late Cretaceous. Science 322, 934–938. http://dx.doi.org/10.1126/science.1162921.
Mpodozis, C., Ramos, V.A., 1989. The Andes of Chile and Argentina. In: Ericksen, G.E., Cañas Pinochet, M.T., Reinemund, J.A. (Eds.), Geology of the Andes and its Relation to Hydrocarbon and Mineral Resources. Earth Science Series, vol. 11. Circum-Pacific Council for Energy and Mineral Resources, pp. 59–90.
Marengo, H.G., 2006, Micropaleontología y estratigrafía del Mioceno marino de la Argentina: Las Transgresiones de Laguna Paiva y del "Entrerriense-Paranense", Tomo 1. Unpublished PhD thesis, Universidad de Buenos Aires, Argentina, p. 124.
Martinod, J., Espurt, N., Brusset, S., Funiciello, F., Faccenna, C., Baby, P., 2008. Dynamic topography into the Amazonian basin: insights from 3-D analogue modeling. In: 7th International Symposium on Andean Geodynamics (ISAG, Nice), Extended Abstracts, pp. 322–325.
Mathalone, J.M.P., Montoya, R.,M., 1995. Petroleum Geology of the sub-Andean basins of Peru. In: Tankard, A.J., Suarez, S.,R., Welsink, H.J. (Eds.), Petroleum Basins of South America: American Association of Petroleum Geologists Memoir, vol. 62, pp. 423–444.
Mégard, F., 1984. The Andean orogenic period and its major structures in central and northern Peru. Journal of the Geological Society of London 141, 893–900.
Mégard, F., 1987. Cordilleran Andes and Marginal Andes: a review of Andean geology north of the Arica Elbow (18°S). In: Monger, J.W.H., Francheteau, J. (Eds.), Circum-pacific Orogenic Belts and Evolution of the Pacific Ocean Basin. American Geophysical Union. Geological Society of America, Geodynamic Series, vol. 18, pp. 71–95.
Miller, M.S., Becker, T.W., 2012. Mantle flow deflected by interactions between subducted slabs and cratonic keels. Nature Geosciences 5, 726–730.
Miller, M.S., Levander, A., Niu, F., Li, A., 2009. Upper mantle structure beneath the Caribbean-South American plate boundary from surface wave tomography. Journal of Geophysical Research 114, B01312. http://dx.doi.org/10.1029/2007JB005507.
Mitrovica, J.X., Beaumont, C., Jarvis, G.T., 1989. Tilting of the continental interior by the dynamical effects of subduction. Tectonics 8, 1079–1094.
Morgan, W., 1965. Gravity anomalies and convection currents. Journal of Geophysical Research 70, 6175–6187. http://dx.doi.org/10.1029/JZ070i024p06175.
Molnar, P., England, P., 1990. Late Cenozoic uplift of mountain ranges and global climate change: chicken or egg? Nature 346, 29–34.
Moucha, R., Forte, A.M., 2011. Changes in African topography driven by mantle convection. Nature Geoscience. http://dx.doi.org/10.1038/ngeo1235.
Müller, R.D., Sdrolias, M., Gaina, C., Roest, W.R., 2008. Age, spreading rates and spreading asymmetry of the world's ocean crust. Geochemistry, Geophysics, Geosystems 9, Q04006. http://dx.doi.org/10.1029/2007GC001743.
Nágera, J.J., 1927. Doctrina del Mar Libre. Universidad de Buenos Aires.
Parras, A., Griffin, M., Feldmann, R., Casadío, S., Schweitzer, C., y Marenssi, S.A., 2008. Correlation of marine beds based on Srand Ar – date determinations and faunal affinities across the Paleogene/Neogene boundary in southern Patagonia, Argentina. Journal of South American Earth Sciences 26, 204–216.
Passalacqua, H., Fernandez, F., Gou, Y., Roure, F., 1995. Crustal architecture and strain partitioning in the Eastern Venezuelan Ranges. In: Tankard, A.J., Suarez-Soruco, R., Welsink, H.J. (Eds.), Petroleum Basins of South America: AAPG Memoir, vol. 62, pp. 667–680.
Pedoja, K., Husson, L., Regard, V., Cobbold, P.R., Ostanciaux, E., Johnson, M.E., Kershaw, S., Saillard, M., Martinod, J., Furgerot, L., Weill, P., Delcaillau, B., 2011. Relative sea-level fall since the last interglacial stage: are coasts uplifting worldwide? Earth Science Reviews. http://dx.doi.org/10.1016/j.earscirev.2011.05.002.
Pysklywec, R.N., Mitrovica, J.X., 1999. The role of subduction-induced subsidence in the evolution of the Karoo Basin. Journal of Geology 107, 155–164.
Ramos, V.A., 1989. Andean foothills structures in northern Magallanes Basin, Argentina. AAPG Bulletin 73 (7), 887–903.
Ramos, V.A., 2005. Seismic ridge subduction and topography: foreland deformation in the Patagonian Andes. Tectonophysics 399 (1–4), 73–86.
Ramos, V.A., 2009. Anatomy and global context of the Andes: main geologic features and the Andean orogenic cycle. In: En Kay, S.M., Ramos, V.A., y Dickinson, W. (Eds.), Backbone of the Americas: Shallow Subduction, Plateau Uplift, and Ridge and Terrane Collision. Geological Society of América, Memoir, vol. 204, pp. 31–65.
Ramos, V.A., y Kay, S.M., 1992. The Southern Patagonian plateau basalts: retroarc testimony of a ridge collision, Argentina. Tectonophysics 205, 261–282.
Ramos, V.A., Cristallini, E.O., y Pérez, D.J., 2002. The Pampean flat-slab of the central Andes. Journal of South American Earth Sciences 15, 59–78.
Räsänen, M., Salo, J.S., Jungnert, H., Romero Pittman, L., 1990. Evolution of the western Amazon lowland relief: impact of Andean foreland dynamics. Terra Nova 2, 320–332.
Regard, V., Lagnous, R., Espurt, N., Darrozes, J., Baby, P., Roddaz, M., Calderon, Y., Hermoza, W., 2009. Geomorphic evidence for recent uplift of the Fitzcarrald Arch (Peru): a response to the Nazca Ridge subduction. Geomorphology v. 107, 107–117.
Ricard, Y., Chambat, F., Lithgow-Bertelloni, C., 2006. Gravity observations and 3D structure of the Earth. Comptes Rendus de l'Acad (c)mie des Sciences. Comptes Rendus Geoscience 338, 992–1001.
Ricard, Y., Richards, M., Lithgow-Bertelloni, C., LeStunff, Y., 1993. A geodynamical model of mantle density heterogeneity. Journal of Geophysical Research 98, 21895–21909.
Richards, M.A., Hager, B.H., 1984. Geoid anomalies in a dynamic earth. Journal of Geophysical Research 89, 5987–6002.
Roure, R., Carnavalli, J.O., Gou, Y., Subieta, T., 1994. Geometry and kinematics of the north Monagas thrust belt, Venezuela. Marine and Petroleum Geology 11, 347–359.
Ruskin, B.G., Dávila, F.M., Hoke, G.H., Jordan, T.E., Astini, R.A., Alonso, R., 2011. Stable isotope composition of Middle Miocene carbonates of the Frontal Cordillera and

Sierras Pampeanas: did the Paranaense seaway flood western and central Argentina? Palaeogeography, Palaeoclimatology, Palaeoecology 308, 293–303.
Russo, R.M., Speed, R.C., Okal, E.A., Shepherd, J.B., Rowley, K.C., 1993. Seismicity and tectonics of the southeastern Caribbean. Journal of Geophysical Research 98 (B8), 14,299–14,319.
Russo, R.M., VanDecar, J.C., Comte, D., Mocanu, V.I., Gallego, A., Murdie, R.E., 2010. Subduction of the Chile ridge: upper mantle structure and flow. GSA Today 20 (9), 4–10.
Shephard, G.E., Liu, L., Gurnis, M., Muller, R.D., 2010. Miocene drainage reversal of the Amazon River driven by plate-mantle interaction. Nature Geoscience 3, 870–875.
Shephard, G.E., Liu, L., Müller, D., Gurnis, M., 2012. Dynamic topography and anomalously negative residual depth of the Argentine Basin. Gondwana Research 22, 658–663.
Spasojevic, S., Liu, L., Gurnis, M., Muller, R.D., 2008. The case for dynamic subsidence of the United States east coast since the Eocene. Geophysical Research Letters 35, L08305. http://dx.doi.org/10.1029/2008GL033511.
Steinberger, B., 2007. Effect of latent heat release at phase boundaries on flow in the Earth's mantle, phase boundary topography and dynamic topography at the Earth's surface. Physics of the Earth and Planetary Interiors 164, 1–2. 2-20.
Stixrude, L., Lithgow-Bertelloni, C., 2005. Thermodynamics of mantle minerals: 1. Physical properties. Geophysical Journal International 162, 610–632.
Strecker, M.R., Alonso, R., Bookhagen, B., Carrapa, B., Coutand, I., Hain, M.P., Hilley, G.E., Mortimer, E., Schoenbohm, L., Sobel, E.R., 2009. Does the topographic distribution of the central Andean Puna Plateau result from climatic or geodynamic processes? Geology 37, 643–646.
Tackley, P.J., Stevenson, D.J., Glatzmaier, G.A., Schubert, G., 1993. Effects of an endothermic phase transition at 670km depth on a spherical model of convection in the Earth's mantle. Nature 361, 699–704.
Tassara, A., Swain, C., Hackney, R., Kirby, J., 2007. Elastic thickness structure of South America estimated using wavelets and satellite-derived gravity data. Earth Planetary Science Letters 253, 17–36.
Turcotte, D., Schubert, G., 2002. Geodynamics. Cambridge University Press.
Walcek, A.A., Hoke, G.D., 2012. Surface uplift and erosion of the southernmost Argentine Precordillera. Geomorphology 153–154, 156–168.
Watts, A.B., 2001. Isostasy and Flexure of the Lithosphere. Cambridge University Press, Cambridge, New York, Melbourne, p. 458.
Winterbourne, J., Crosby, A., White, N.J., 2009. Depth, age and dynamic topography of oceanic lithosphere beneath heavily sedimented Atlantic margin. Earth and Planetary Science Letters. ISSN: 0012-821X 287 (1–2). ISSN: 0012-821X, 137–151.
Yañez, G.A., Ranero, C.R., von Huene, R., Diaz, J., 2001. Magnetic anomaly interpretation across the southern central Andes (32°–34°S): the role of the Juan Fernández Ridge in the late Tertiary evolution of the margin. Journal of Geophysical Research 106, 6325–6345.